Atomistic simulations of nanostructure and dynamics of phosphoric acid-benzimidazole systems: A fuel cell initiative

A

thesis submitted

in partial fulfillment of the requirements for the degree of

DOCTOR OF PHILOSOPHY

by

Minal Sachin Pednekar

Roll No.:20093045

Indian Institute of Science Education and Research, Pune

2016

Certificate

Certified that the work incorporated in the thesis entitled *"Atomistic simulations of nanostructure and dynamics of phosphoric acid-benzimidazole systems: A fuel cell initiative"* submitted by **Minal Sachin Pednekar** was carried out by the candidate, under my supervision. The work presented here or any part of it has not been included in any other thesis submitted previously for the award of any degree or diploma from any other University or institution.

Date:

Dr. Arun Venkatnathan

(Supervisor)

Declaration

I declare that this written submission represents my ideas in my own words and where others ideas have been included, I have adequately cited and referenced the original sources. I also declare that I have adhered to all principles of academic honesty and integrity and have not misrepresented or fabricated or falsified any idea/data/fact/source in my submission. I understand that violation of the above will be cause for disciplinary action by the Institute and can also evoke penal action from the sources which have thus not been properly cited or from whom proper permission has not been taken when needed.

Date:

Minal Sachin Pednekar

(Roll No.:20093045)

I dedicate this thesis to my family...

Acknowledgement

I deeply acknowledge Indian Institute of Science Education and Research (IISER), for providing an excellent research facility and graduate fellowship for my research work. I thank Prof. K. N. Ganesh (Director, IISER, Pune) for excellent facilities. I express my sincere gratitude to my thesis advisor Dr. Arun Venkatnathan for his continuous support during my Ph.D program, for his patience, motivation, encouragement and immense knowledge. His guidance helped me to develop an understanding of the subject and in writing of this thesis.

I am grateful to my Research Advisory Committee members Dr. Arun Venkatnathan, Dr. Sreekumar Kurungot and Dr. Prasenjit Ghosh for their insightful comments and encouragement.

I thank Anurag for the collaborative work. I thank Praveen and Prabhat for proof reading this thesis. I thank Wilbee for being a great support and constantly motivating me during my research work. I express my sincere thanks to Ramya, Rakesh and Meghna for their help and support. I thank Reman and Hridya and my all computational colleagues for their suggestions and comments during my presentation. I thank IT staff, Neeta, Suresh, Sachin and Abhijeet for providing technical support.

Last, but not the least I would like to thank all my family members without whom it was impossible for me to strive towards my goals. I am deeply grateful to my mom and dad for their love and spiritually supporting me throughout my PhD work and life. Words cannot express how grateful I am to my brother Atul, sister-in-law Shubhangi, Parth, Samit and my parents-in-laws for their support and for all of the sacrifices that they have made on my behalf. In the end I would like to express my appreciation for the love and support given by my husband at every step of my research work.

IISER, PUNE **Minal Sachin Pednekar**

List of Publications

- Pahari, S.; Choudhury, C.; Pandey, P.; **More, M.**; Venkatnathan, A.; Roy, S.; *Molecular Dynamics Simulation of phosphoric acid doped monomer of polybenzimidazole: A potential component polymer electrolyte Membrane of Fuel Cell*, J. Phys. Chem. B *2012*, 116, 7357-7366.

- **More, M.**; Pahari, S.; Roy, S.; Venkatnathan, A.; *Characterization of the structures and dynamics of phosphoric acid doped benzimidazole mixtures: a molecular dynamics study*, J. Molecular Modeling *2013*, 19, 109-118.

- Sunda, A.; **More, M.**; Venkatnathan, A.; *A Molecular Investigation of structure and dynamics of the Phosphoric/Triflic acid blends of ABPBI (2,5-Benzimidazole) Polymer Electrolyte Membrane*, Soft Matter *2013*, 9, 1122-1132.

- **More, M.**; Sunda A.; Venkatnathan, A.; *Polymer chain length, phosphoric acid doping and temperature dependence on structure and dynamics of an ABPBI [poly(-2,5-benzimidazole)] polymer electrolyte membrane*, RSC Advances *2014*, 4, 19746-19755.

Contents

List of Figures

List of Tables

Abbreviations

ABPBI	:	Poly(2,5-benzimidazole)
OPLS-AA	:	Optimized Potentials for Liquid Simulations-All Atom
PA	:	Phosphoric Acid
PFSA	:	Perfluorosulfonic Acid
PME	:	Particle-Mesh Ewald
MD	:	Molecular Dynamics
MSD	:	Mean Square Displacement
NPT	:	Isobaric Isothermal
NVT	:	Isochoric Isothermal
RDF	:	Radial Distribution Function
TFA	:	Trifluoromethanesulfonate or Triflate ion

Abstract

Phosphoric acid doped benzimidazole membranes like poly[2,2-(m-phenylene)-5,5-bibenzimidazole] (PBI) and poly(2,5-benzimidazole) (ABPBI) have been investigated as fuel cell electrolytes to operate at elevated temperatures. Several experimental studies have synthesized and characterized various physical, chemical and electrochemical properties of these phosphoric acid doped benzimidazole systems. In this thesis, computer simulation methods such as Molecular Dynamics is employed to examine structural and dynamical properties of phosphoric acid-benzimidazole systems. The insights from computation can spur further experimental investigations on fuel cell membranes for anhydrous proton conduction. Since, benzimidazole moiety is an important constituent of these membranes, the interactions in phosphoric acid-benzimidazole mixtures is first examined. The structural properties (Radial Distribution Function), dynamical properties (diffusion) and hydrogen bond lifetime calculations allude to the possibility that benzimidazole and phosphoric acid molecules exhibit dual proton-acceptor/donor functionality.

A subsequent examination of interactions between phosphoric acid and ABPBI shows that the inter-chain and intra-chain interactions in ABPBI membrane remain unaffected with chain length and temperature. However, these interactions are significantly changed with phosphoric acid doping. The radius of gyration is found to increase linearly with increasing ABPBI chain length but remains invariant to phosphoric acid doping and temperature. The end-to-end distance deviates from linearity with chain length of ABPBI which suggests increased coiling of membrane (independent of phosphoric acid doping and temperature). The diffusion coefficient of phosphoric acid increases with phosphoric acid doping and temperature, but remains constant with polymer chain length. The activation energy of diffusion of phosphoric acid decreases significantly with an increase in polymer chain length at low phosphoric acid doping, but remains unaffected at higher phosphoric acid doping.

Chapter 1

Introduction

1.1 Polymer Electrolyte Membranes

Polymer Electrolyte Membrane Fuel Cells (PEMFC) have attracted interest due to their ability to provide clean energy and high power density for a variety of stationary and mobile applications.[1,2] Hydrogen gas is fed at the anode where it dissociates into protons

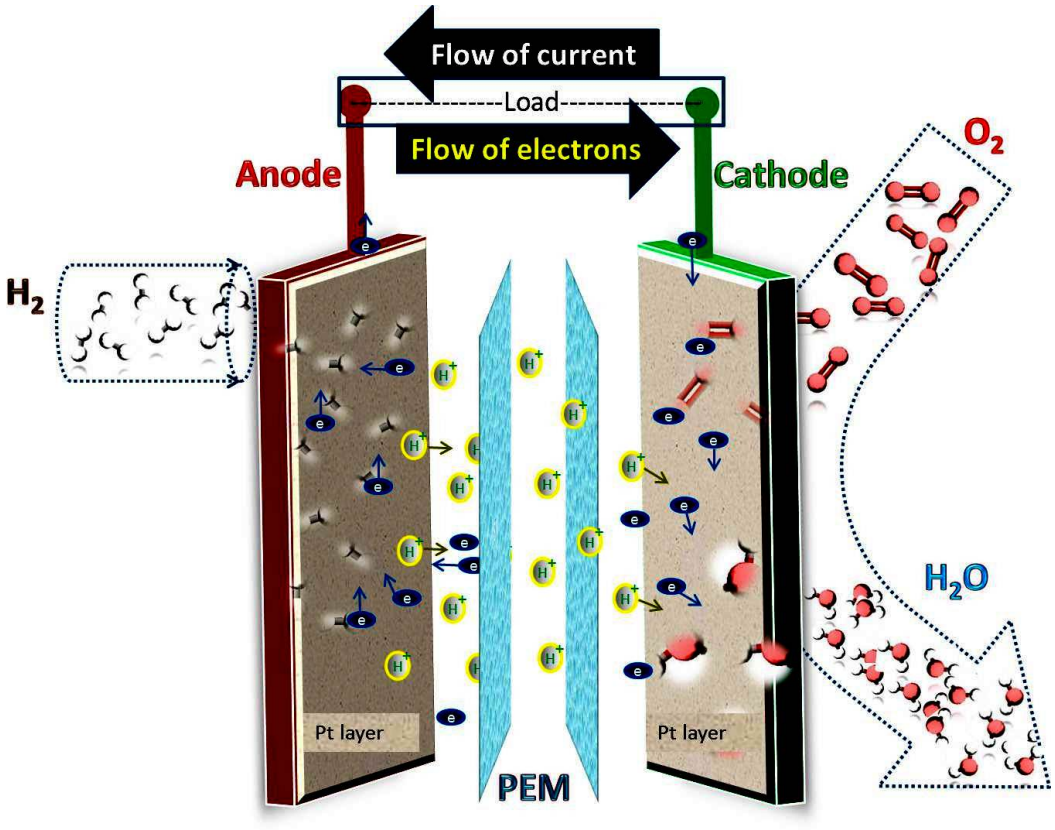

Figure 1.1: Schematic of PEMFC.

and electrons in the presence of a platinum catalyst. While the electrons flow through the

external circuit, the protons are transported via the electrolytic medium to the cathode. Oxygen gas fed via the cathode associates with protons and electrons to produce liquid water. The reactions can be summarized as:

Anode:

$$H_2 \rightarrow 2H^+ + 2e^- \tag{1.1}$$

Cathode:

$$\frac{1}{2}O_2 + 2H^+ + 2e^- \rightarrow H_2O \tag{1.2}$$

Overall Reaction:

$$H_2 + \frac{1}{2}O_2 \rightarrow H_2O \tag{1.3}$$

The polymer membrane is an important component of the PEMFC (see Figure 1.1) due to its role in proton conduction between the electrodes. The key requirements of a polymer membrane to serve as an electrolyte are: thermal and mechanical stability, chemical resistivity, inhibiting fuel cross-over across electrodes, reduction of CO poisoning of the catalyst, and high proton conduction under prolonged fuel cell operation.[3–5] Several classes of polymer membranes like the perfluorosulfonic acid (PFSA) membranes (see Figure 1.2),[3–7] cross-linked sulfonated poly(1,3-cyclohexadiene)[8,9] and aromatic membranes like Polyetherketones[6,7] and Polybenzimidazole[10] have been considered as electrolytes which satisfy these requirements. Among them, PFSA membranes like Dow, Aciplex and Nafion have been extensively investigated by experiments and theoretical methods.[11–20] While, PFSA membranes offer high conductivity, their efficiency depend on the amount of humidification and fuel cell operating temperature. Hence, the use of PFSA membranes remains limited to 100 °C, due to their dependence on water for proton transport. Further, operation of fuel cells using the membranes as electrolytes at T $>$ 100 °C leads to an increase in CO poisoning of the catalyst layer. As an alternative to PFSA membranes, cost effective benzimidazole-based membranes like poly[2,2-(m-

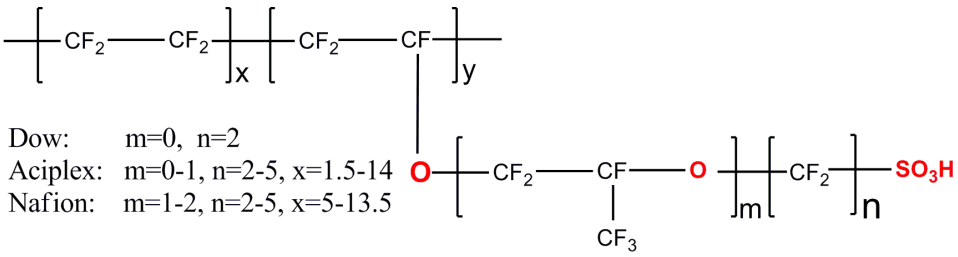

Figure 1.2: Chemical structure of PFSA polymer membrane.

phenylene)-5,5-bibenzimidazole] (PBI)[21] and poly(2,5-benz-imidazole) (ABPBI)[22] have been developed as fuel cell electrolytes and tested up to 200 °C.[10,23–27] These membranes when doped with phosphoric acid (PA)[28] serves as a replacement of water for transport of protons at elevated temperatures.[29,30] ABPBI membrane have received recent attention due to equivalent or better electrochemical properties compared to PBI.[22,31–40] Chemically, a monomer unit of the ABPBI membrane consists of a single imidazole ring with two nitrogen atoms that serves as a proton acceptor[41] as well as proton donor depending the pH level[42] and can interact with an acid like PA. Due to the absence of the phenylene ring in ABPBI, ABPBI has higher concentration of benzimidazole groups compared to PBI per repeat unit of polymer (or polymer weight). Hence, ABPBI can absorb more acid than PBI (especially at higher acid concentration) and has higher affinity towards PA. PA-doped ABPBI membranes were shown[43] to display better conductivity and higher thermal stability than the corresponding PA-doped PBI membrane.

Asensio et al.[31] employed Fourier transform Infrared Spectroscopy on PA doped ABPBI membranes and reported a maximum conductivity of 6.2×10^{-2} S cm^{-1} at 150 °C and 30% Relative Humidity. The authors also concluded that the nitrogen (N–H) of ABPBI serves as a proton donor. The authors observed the formation of $H_2PO_4^-$ anions (see Figure 1.3), suggesting that proton transfer occurs via a Grotthuss[44] mechanism. Subsequently, Asensio et al.[35] also showed that PA-doped ABPBI membranes exhibit high proton conductivity, similar to PA-doped PBI membranes. Kim et al.[32] showed that the

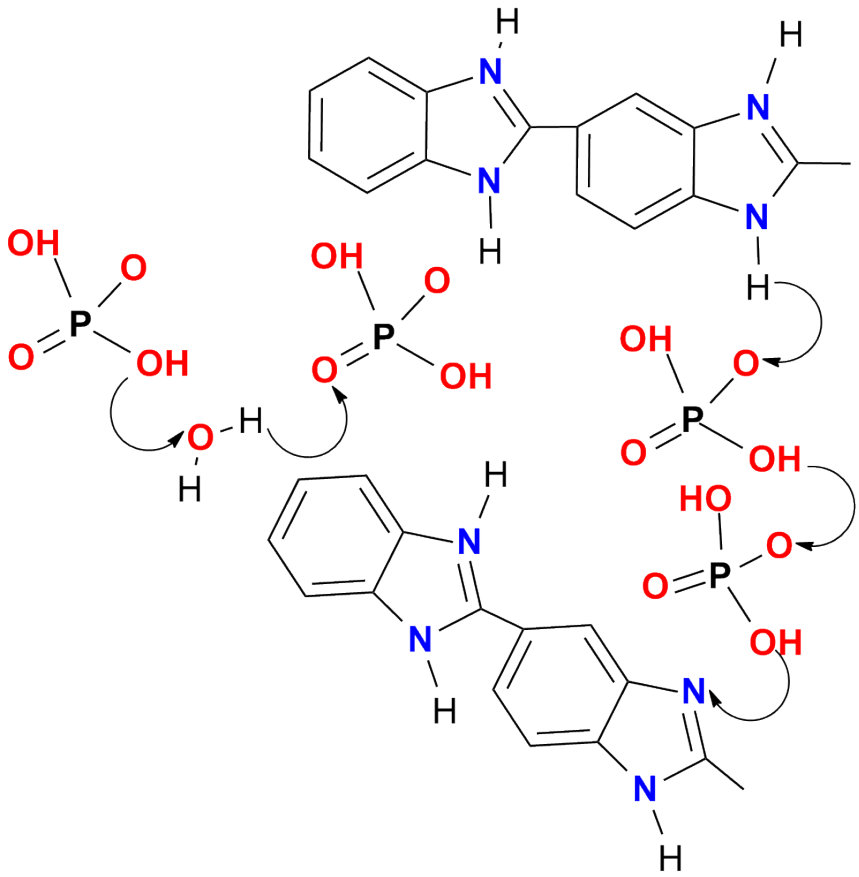

Figure 1.3: Proton conduction in phosphoric acid doped polybenzimidazole (Adapted from Asensio et al.[22] with permission of The Royal Society of Chemistry).

ABPBI membrane can be easily synthesized from 3,4-diaminobenzoic acid (DABA). Krishnan et al.[36] reported a conductivity of 2.6×10^{-2} S cm^{-1} at 180 °C when 1.2 molecules of PA were doped per monomer unit of ABPBI. The authors concluded that the poisoning of CO was limited, even beyond 170 °C. Wannek et al.[38] also demonstrated that PA-doped ABPBI membranes work efficiently during prolonged fuel cell operation. Diaz et al.[45] investigated the role of temperature on PA uptake by the ABPBI membrane and found that low temperature casting results in higher uptake of PA due to less compact supra-molecular packing and large number of accessibility of sorption sites. Linares et al.[46] characterized physico-chemical properties of ABPBI membranes at varying amount

of PA doping. The authors observed suitable mechanical strength, low acid leaching rate, good electrochemical stability and excellent thermal stability even beyond 500 °C. Conti et al.[47] observed hydrogen bond interactions between PA and ABPBI using FT-Raman spectroscopy. The interactions between PA and ABPBI were also examined by Giffin et al.[42] using FT-ATR-IR. The authors concluded that proton exchange occurs between the imidazole moieties of the polymer chain and phosphoric acid leading to the formation of dihydrogen phosphate ions and protonated imidazolium cations.

While a large body of experimental work have been reported on PA doped benzimidazole systems, computational investigations have been very scarce. Li et al.[48] examined interaction in hydrated and PA doped ABPBI, PBI and poly(p-phenylene benzobisimidazole) (PBDI) membranes using MD simulations. The authors used MD simulations to show that ABPBI has a higher affinity for PA than PBI does. Further, the authors concluded that the protonated oxygen atom of PA acts as a strong hydrogen acceptor. Due to the limited theoretical studies so far, this thesis will offer an in-depth investigation into molecular interactions between phosphoric acid and benzimidazole systems using classical MD simulations. The description of force field and other theoretical principles involved in molecular mechanics and MD simulations is seen in Allen et al[49] and Leach et al.[50] A concise discussion on force fields and simulation protocol is described in the next section.

1.2 Force Field and simulation protocol

The force field can be described as a total potential energy (V_{total}) of a chemical system and is defined as:

$$V_{total} = \underbrace{V_{bonds} + V_{angles} + V_{torsion}}_{V_{bonded}} + \underbrace{V_{electrostatic} + V_{vdw}}_{V_{non-bonded}} \tag{1.4}$$

$$V_{bonded} = \sum_{bonds} \frac{k_b}{2}(r - r_0)^2 + \sum_{angle} \frac{k_\theta}{2}(\theta - \theta_0)^2 + \sum_{torsion}^{n=0-5} C_n(\cos(\psi))^n \quad (1.5)$$

k_b and k_θ are force constants for bonds and angles respectively, r_0 is the equilibrium bond length and θ_0 is the equilibrium bond angle. C_n is called the torsional coefficient, ψ = ϕ-180°, where ψ is a torsion angle. The non-bonded potential ($V_{non-bonded}$) energy is defined as:

$$V_{non-bonded} = \sum_{ij} 4\epsilon_{ij} \left[\left(\frac{\sigma_{ij}}{r_{ij}} \right)^{12} - \left(\frac{\sigma_{ij}}{r_{ij}} \right)^{6} \right] + \frac{1}{4\pi\epsilon_0} \frac{q_i q_j}{\epsilon_r r_{ij}} \quad (1.6)$$

where, ϵ_{ij} is the depth of potential well, r_{ij} is the distance between atoms, σ_{ij} is the distance at which potential energy is zero, q_i and q_j are the charges on atom i and j. ϵ_r is the dielectric constant and ϵ_0 is permittivity of vacuum. The parameters in this force-field equation are obtained from experiments or quantum chemistry calculations. The commonly used software force-field parameters for molecules, macromolecular and biological systems are: CHARMM,[51] AMBER,[52] OPLS-AA,[53] etc.

A schematic diagram of MD simulation protocol is shown in Figure 1.4. The first step of the simulation is design of input or initial configurations of a chemical system. The design principle to create configurations is derived from experimental work such as crystal structure and/or density. Molecular builders like MOLDEN[54] or Gaussview[55] are used for generation of initial configurations. The configurations were visualized using Visual Molecular Dynamics (VMD)[56] and Chimera[57] program. The configurations are represented in Cartesian or internal coordinates (Z-matrix) format. The second step is an energy minimization of the configuration using a steepest descent algorithm[58] to remove any unfavorable interactions. The energy minimized structure was used for simulated annealing. The annealing process involves periodic heating and cooling of the configurations to obtain a reasonable starting density to mimic experimental densities. The well annealed configurations were used as inputs for equilibration followed by production runs.

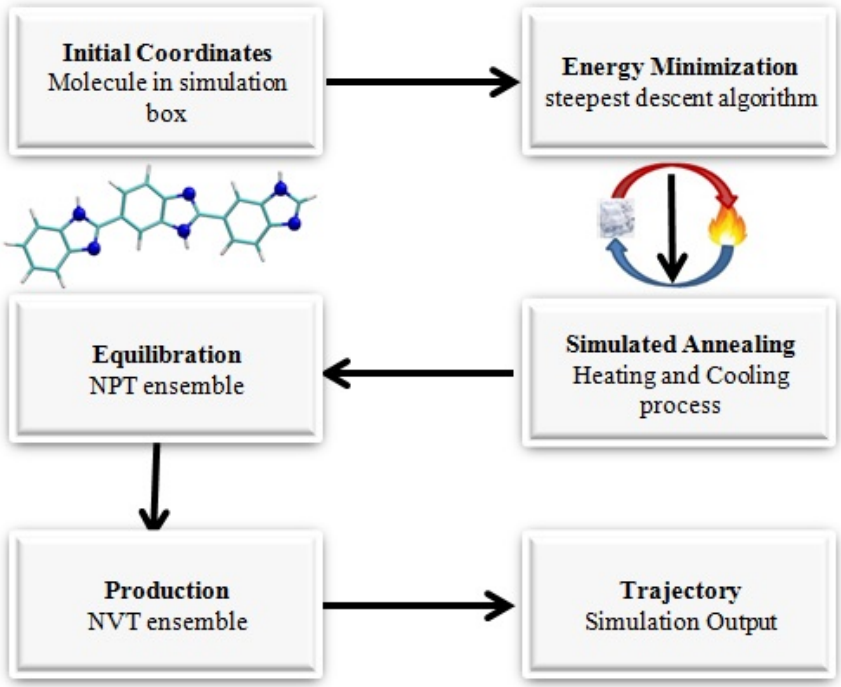

Figure 1.4: A schematic MD simulation protocol

The trajectories from the production runs were analyzed to calculate various structural and dynamical properties presented in the next section.

1.3 Analysis

1.3.1 Radial Distribution Function

The structural properties is characterized using Radial Distribution Functions (RDFs).[49] The RDF ($g_{AB}(r)$) can be calculated as:

$$g_{AB}(r) = \frac{1}{\langle \rho_B \rangle_{local}} \frac{1}{N_A} \sum_{i \in A}^{N_A} \sum_{i \in B}^{N_B} \frac{\delta(r_{ij} - r)}{4\pi r^2} \tag{1.7}$$

where, N_A and N_B is the number of *A* and *B* particles respectively, r_{ij} is the distance between i^{th} and j^{th} particle, $\langle \rho_B \rangle_{local}$ is the particle density of type B at a distance r, averaged over all spheres around particles A.

1.3.2 Mean Square Displacement

The Mean Square Displacement (MSD) is calculated using the Einstein equation[49] and is written as :

$$\lim_{(t\to\infty)} \langle \|r_i(t) - r_i(0)\|^2 \rangle_{i\in A} = 6D_A t \tag{1.8}$$

where, r_i is the center-of-mass position of any molecule, $r_i(0)$ and $r_i(t)$ are positions of atoms at time *t* = 0 and *t* respectively. D_A is the self-diffusion coefficient calculated from the linear regime of the corresponding MSD.

1.3.3 Activation Energy

The energy of activation (E_A) of diffusion is calculated from the diffusion coefficient (D_A) using an Arrhenius equation and is written as:

$$\ln D_A = \ln\ D_0 - \frac{E_\mathrm{A}}{RT} \tag{1.9}$$

where, D_0 is pre-exponential factor, *R* is gas constant and *T* is temperature.

1.3.4 Radius of Gyration

The radius of gyration of a polymer chain[59,60] is written as:

$$R_g = \left(\frac{\sum_i \|r_i\|^2 m_i}{\sum_i m_i} \right)^{\frac{1}{2}} \tag{1.10}$$

where, m_i is the mass of atom i, r_i is the position of atom i with respect to the center of mass of the polymer chain.

1.4 Scope of this thesis

Chapter 2 describes the interactions between benzimidazole (BI) with varying PA concentrations using classical MD simulations. The effect of initial configuration on structural and dynamical properties with varying PA doping level is discussed. The influence of PA uptake on intermolecular interactions between BI and PA, the mobility of BI and PA and hydrogen bond dynamics in PA doped BI mixtures are also investigated.

Chapter 3 describes the effect of polymer chain length and temperature on structure and dynamics of PA doped ABPBI membrane. The intra and inter chain interactions are examined using RDFs. The effect of phosphoric acid doping and polymer chain length on radius of gyration, end-to-end polymer chain distance, phosphoric acid clustering and diffusion of phosphoric acid is also calculated.

Chapter 4 presents salient findings from previous chapters with a short discussion on Protic Ionic Liquids as alternative materials for proton conduction.

Chapter 2

Structure and Dynamics of phosphoric acid–benzimidazole mixtures

2.1 Introduction

In this chapter, the various interactions of a benzimidazole (BI) molecule (a monomer unit of the ABPBI polymer membrane) with PA with varying PA doping is examined. The results obtained from this study are important as they lead to a better understanding of the participation of the amine hydrogen of BI in hydrogen bonding with PA, and of the hydrogen-bonding interactions that occur between BI and PA molecules at various PA dopant levels. The details of MD simulations are described in Section 2.2. The results of MD simulations are discussed in Section 2.3. The summary of key findings concludes this chapter.

2.2 Computational details

All MD simulations were performed using the GROMACS[61] 4.0.7 program. The chemical structure of BI and PA molecule are shown in Figure 2.1. The force-field parameters for BI were taken from the OPLS-AA force-field database,[62] whereas the force-field parameters for PA were extracted from the work of Spieser et al.[63] Two configurations containing 1,000 molecules of neat BI and neat PA were initially constructed. The resulting config-

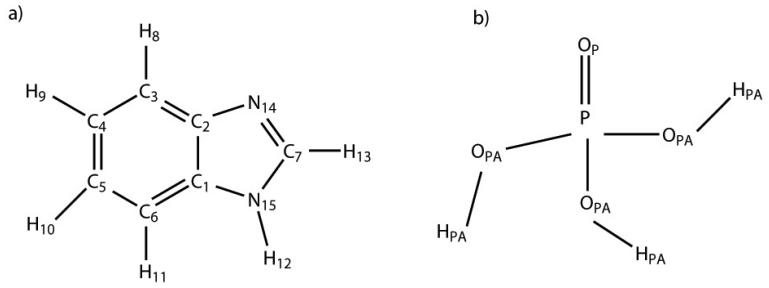

Figure 2.1: Chemical structure of a) BI and b) PA. (The atom types of these structures are used in RDFs and hydrogen bonds).

urations were energy minimized using the steepest descent algorithm.[58] The minimized energy configurations of neat BI and neat PA were chosen as input for a subsequent equilibration. Various PA-doped BI mixtures were created by doping with different amounts of PA. In order to describe the compositions of these mixtures, parameter γ has been defined which denotes the number of PA molecules for each BI molecule present in the mixture.

To check the effect of the initial configuration on the structural and dynamic properties of the mixtures, PA-doped BI mixtures were created using grid and solvated methods. The construction of input configurations using grid and solvated methods is now described using $\gamma = 2$ as an example. The grid method (denoted by the letter "g" in tables and figures) consisted of arranging one BI molecule and two PA molecules regularly in a cubic box, and the process was repeated until a configuration containing 64 BI molecules and 128 PA molecules was obtained (see Figure 2.2a). The solvated method (denoted by the letter "s" in tables and figures) was implemented by creating a configuration containing 64 BI molecules and subsequently solvating with 128 PA molecules, as seen in Figure 2.2b. Using the grid and solvated methods, configurations corresponding to γ = 4, 8, and 12 were generated and subsequently energy-minimized. The energy-minimized configuration was used as an input for the simulated annealing. Using a timestep of 2 fs and the NPT ensemble, a simulated annealing method for each γ was performed, as follows: Each

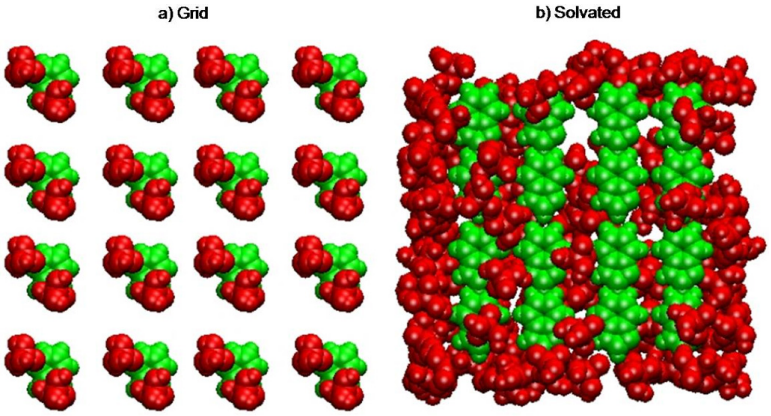

Figure 2.2: Initial configuration of γ = 2 (green = BI, red = PA) using a) grid and b) solvated methods.

configuration was heated from 450 K to 660 K and cooled back to 450 K in steps of 30 K, with a total simulation time of 5.2 ns per cycle. The annealing procedure was repeated five times, and the final configuration was chosen as input for a subsequent equilibration.

For all of the MD simulations, the cut-off for van der Waals and electrostatic interactions was chosen as 1.0 nm. The timestep was 1 fs and the leapfrog algorithm[49] was used as an integrator for the equation of motion. Each MD simulation was equilibrated for 10 ns using the NPT ensemble with an isotropic pressure of 1 bar and a Berendsen barostat.[64] Temperature was kept constant using a velocity-rescale thermostat[65] with a coupling time of 0.1 ps. The Particle-Mesh Ewald[66,67] (PME) method was used to calculate long-range electrostatic interactions. Equilibration was followed by a 20 ns production run using the NPT ensemble with the Nosé–Hoover thermostat[68,69] and the Parrinello–Rahman barostat.[70,71] MD equilibration and production runs with neat BI and neat PA were performed from 325 K to 475 K, and with PA-doped BI mixtures at 350 K, 400 K, and 450 K. Trajectories from the production runs were recorded every 5 ps to calculate the density, RDFs, MSD, and the diffusion of each neat system and PA-doped BI mixture.

2.3 Results and Discussion

2.3.1 Densities, structures, and dynamics of the neat systems

As an initial test the properties of neat BI and neat PA were characterized (using MD simulations) and validated with existing experimental/theoretical data. The computed average densities for the neat BI and neat PA as a function of temperature are shown in Figure 2.3. The simulated density (1.14 g cm^{-3}) of neat BI at 325 K is in reasonable agreement with a

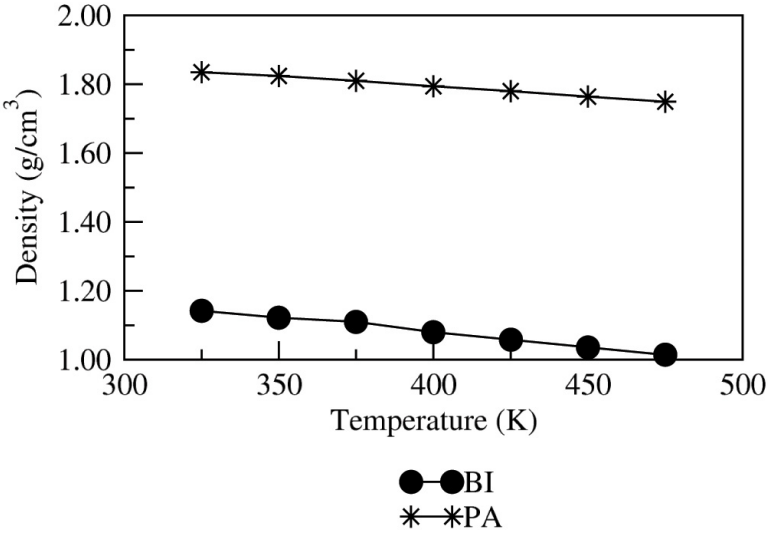

Figure 2.3: Densities of neat Benzimidazole and neat Phosphoric acid.

previously calculated density[72] (1.22 g cm^{-3}) of BI at 298 K. Similarly, the simulated density (1.84 g cm^{-3}) of PA at 325 K is in reasonable agreement with a previously calculated density[63] (1.89 g cm^{-3}) at 300 K, and is in excellent agreement with the experimental density[73] (1.845 g cm^{-3}) at 333 K. The calculated densities of neat BI and neat PA barely change over a wide temperature range (T = 325–475 K). RDFs of the neat BI and neat PA are shown in Figure 2.4. The qualitative features of the RDFs are very similar at all temperatures. The RDFs can be classified based on interactions: intermolecular hydrogen

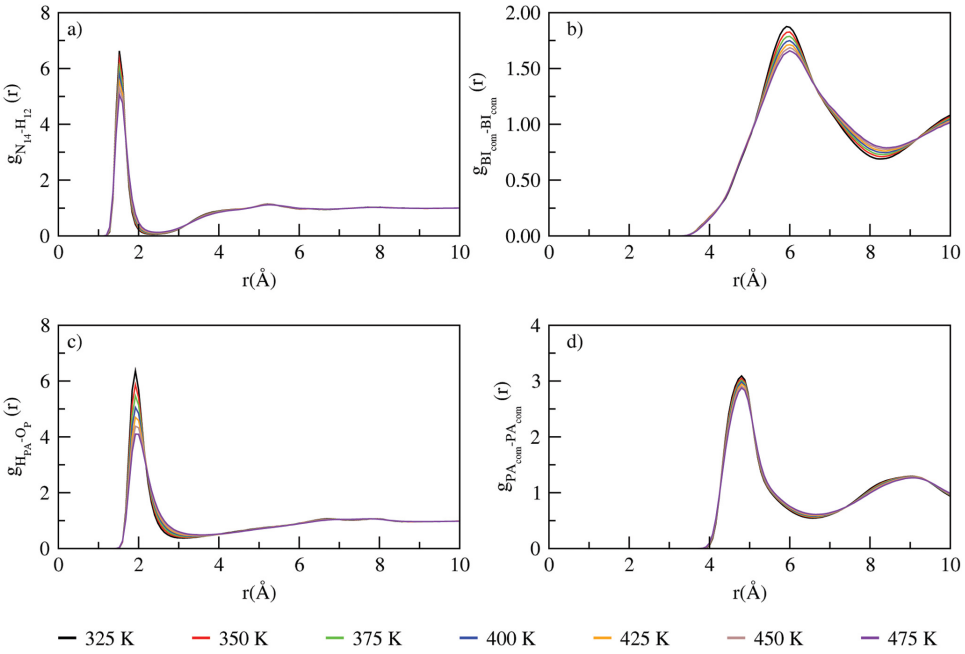

Figure 2.4: RDFs of a) N_{14}-H_{12}, b) BI_{com}-BI_{com}, c) H_{PA}-O_P, and d) PA_{com}-PA_{com}.

bonding between atoms in neat BI and neat PA, and center-of-mass interactions between BI molecules and between PA molecules. For example, the N_{14}–H_{12} RDFs (atom numbers are shown in Figure 2.1) show the presence of intermolecular hydrogen bonding in neat BI. The hydrogenbond lengths are evident from a first peak at 1.6 Å and a minimum at 2.4 Å. An examination of the BI_{com}–BI_{com} RDFs ("com" denotes the center of mass) shows a first minima at 8 Å with a coordination number of 12.5. This large coordination number shows the theoretical maximum number of BI molecules that can exist in the first solvation shell, and also provides a benchmark for comparing BI–BI interactions in PA-doped BI mixtures. The H_{PA}–O_P RDFs in neat PA show strong intermolecular hydrogen bonding between the nonprotonated oxygen (O_P) and hydrogen (H_{PA}). The H_{PA}–O_P RDFs show a first peak at 2 Å, a minimum at 2.8 Å, and are consistent with experimental data.[74] The PA_{com}–PA_{com} RDFs show a first peak at 4.8 Å and agree well with the results reported by Tsuchida.[75] The PA_{com}–PA_{com} RDFs show a first minimum at 6.5 Å, corresponding to a

coordination number of 13.13. This large solvation shell of PA reflects the high density of the system.

The mobilities of neat BI and neat PA are gauged from the MSD (calculated using Eqn. 1.8), where D_A is the corresponding self-diffusion coefficient of either BI or PA, calculated from the linear regime of the corresponding MSD (see Figure B2-1 of Appendix B). As seen from Table 2.1, the diffusion coefficients of neat BI and neat PA increases with temperature. The increase in the diffusion coefficient is larger for PA than for BI. The diffusion coefficients calculated in this work for different temperatures were compared with the diffusion in PA-doped BI mixtures. The diffusion of neat PA calculated in

Table 2.1: Diffusion coefficients ($\times 10^{-7}$ cm^2 s^{-1}) obtained for neat BI and neat PA.

T (K)	BI	PA
325	4.95	0.06
350	16.10	0.26
375	33.85	0.68
400	57.51	1.81
425	93.22	3.55
450	137.80	6.39
475	198.10	10.70

this work (0.06×10^{-7} cm^2 s^{-1} at 325 K) is in excellent agreement with the simulated diffusion coefficient (0.1×10^{-7} cm^2 s^{-1} at 300 K) reported by Spieser et al.[63] The diffusion of neat PA observed in experimental measurements[29] is 1.75×10^{-7} cm^2 s^{-1} (315 K), and is an order of magnitude larger than the simulated diffusion coefficients. The higher value of the experimental diffusion coefficient is due to the presence of phosphate anions in neat PA. The activation energy for the diffusion of neat PA according to the simulations is 44

kJ mol^{-1}, and is higher than the calculated activation energy of 24 kJ mol^{-1} reported by Li et al.[76] The difference in activation energy between the simulations and the work of Li et al.[76] is due to the choice of force field used in the simulations. This can be seen in the simulated density of Li et al.,[76] which shows a deviation of 12% from the experimental density of PA.

2.3.2 Effect of initial configurations on the structure and dynamics

The computed densities of the PA-doped BI mixtures (from the grid and solvated configurations) at various temperatures based on 10 ns of MD equilibration is shown in Table 2.2. For the grid and solvated configurations, the densities of the PA-doped BI mixtures de-

Table 2.2: Densities (g cm^{-3}) obtained for PA-doped BI mixtures from the grid (g) and solvated (s) configurations

T (K)	$\gamma = 2$		$\gamma = 4$		$\gamma = 8$		$\gamma = 12$	
	g	s	g	s	g	s	g	s
350	1.485	1.483	1.601	1.605	1.696	1.689	1.732	1.734
400	1.454	1.453	1.574	1.573	1.662	1.663	1.703	1.703
450	1.423	1.424	1.541	1.541	1.632	1.633	1.671	1.672

crease linearly with temperature. The differences between the densities (for all γ and T) obtained using the grid configuration and those obtained with the solvated configuration are very insignificant. The structural rearrangements that occur in PA-doped BI mixtures for the grid and solvated configurations can be seen by examining the RDFs between the nitrogen (N_{14} and N_{15}) atoms and the phosphorus (P) atom (shown in Figure 2.5a, 2.5b). The RDFs calculated (for all γ and T) using the grid and solvated configurations show very similar features. The diffusion coefficients calculated (for all γ and T) from the grid

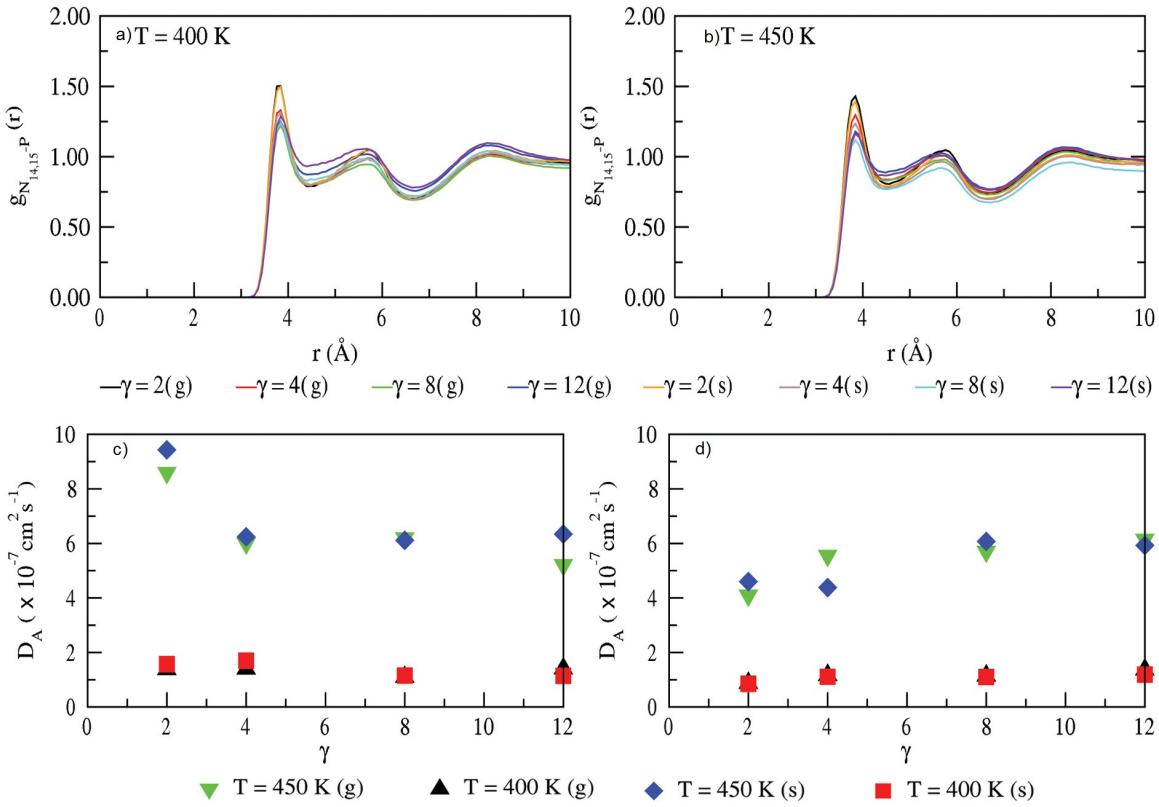

Figure 2.5: $N_{14,15}$-P RDFs obtained from the grid and solvated configuration of a) 400 K and b) 450 K. Diffusion coefficient of c) BI and d) PA at 400 K and 450 K.

and solvated configurations (see Figure 2.5c, 2.5d) are also similar. Hence, a comprehensive examination of the densities, RDFs, and diffusion coefficients obtained using the grid and solvated configurations of PA-doped BI mixtures indicated that the choice of input configuration does not influence any properties. To eliminate any finite-size effect, the configuration corresponding to each γ (obtained from the production run) was replicated twice in each direction of the cubic box. Since, simulations using grid and solvated input configurations showed similar properties, only the solvated configuration were chosen to create the replicated PA doped BI mixtures. The replicated mixture (for each γ) was equilibrated for a further 10 ns. The densities of the replicated mixtures (calculated based on the equilibration runs) are shown in Table A2-1 (see Appendix A). Further, all RDFs,

MSDs, and diffusion coefficients shown in subsequent sections were calculated based on the 20 ns production runs for the replicated mixtures.

2.3.3 Influence of PA uptake on intermolecular interactions

The intermolecular interaction between the imine nitrogen (N_{14}) and the amine hydrogen (H_{12}) in BI (in the PA-doped BI mixtures) can be explored using the N_{14}–H_{12} RDFs shown in Figure 2.6a. The imine nitrogen, which contains a lone pair of electrons, acts as a hydrogen acceptor (via hydrogen bonding) from the amine hydrogen. The first minimum in these RDFs appears at 2.9 Å (for all γ) and corresponds to a coordination number (see Table 2.3) of 0.3 (γ = 2) or 0.05 (γ = 12). This decrease in coordination number shows that the tendency for the imine nitrogen (N_{14}) and amine hydrogen atoms to form a hydrogen bond decreases with increasing γ. Due to the presence of a large number of PA molecules, there is significant separation between any two BI molecules, which shows that the peak height for the length of the hydrogen bond between the N_{14} and H_{12} atoms decreases with γ. The BI_{com}–BI_{com} RDFs presented in Figure 2.6b show a minimum at 8.5 Å , corresponding to a coordination number of 7.75 (γ = 2) or 2.80 (γ = 12). This decrease in coordination number with γ is due to the increasing solvation of the BI molecules by PA. The intermolecular H_{PA}–O_P RDFs in Figure 2.6c show a very sharp peak at 1.5 Å, where there is strong hydrogen bonding, and such observations are consistent with the experimental data of Tromp et al.[74] and the previous results for neat PA reported by Tsuchida.[75] The H_{PA}–O_P RDFs show a first minimum at 2.50 Å corresponding to a coordination number of 0.60 (γ = 2) or 0.75 (γ = 12). The slight increase in coordination number shows that there is marginal increase in intermolecular hydrogen bonding with increasing γ. The PA_{com}–PA_{com} RDFs in Figure 2.6d show a first peak at 4.95 Å and a minimum at 6.5 Å, consistent with the results reported by Tsuchida[75] for neat PA. The coordination number obtained at this minimum in the PA_{com}–PA_{com} RDFs increases from 8.15 (γ = 2) to 12.50

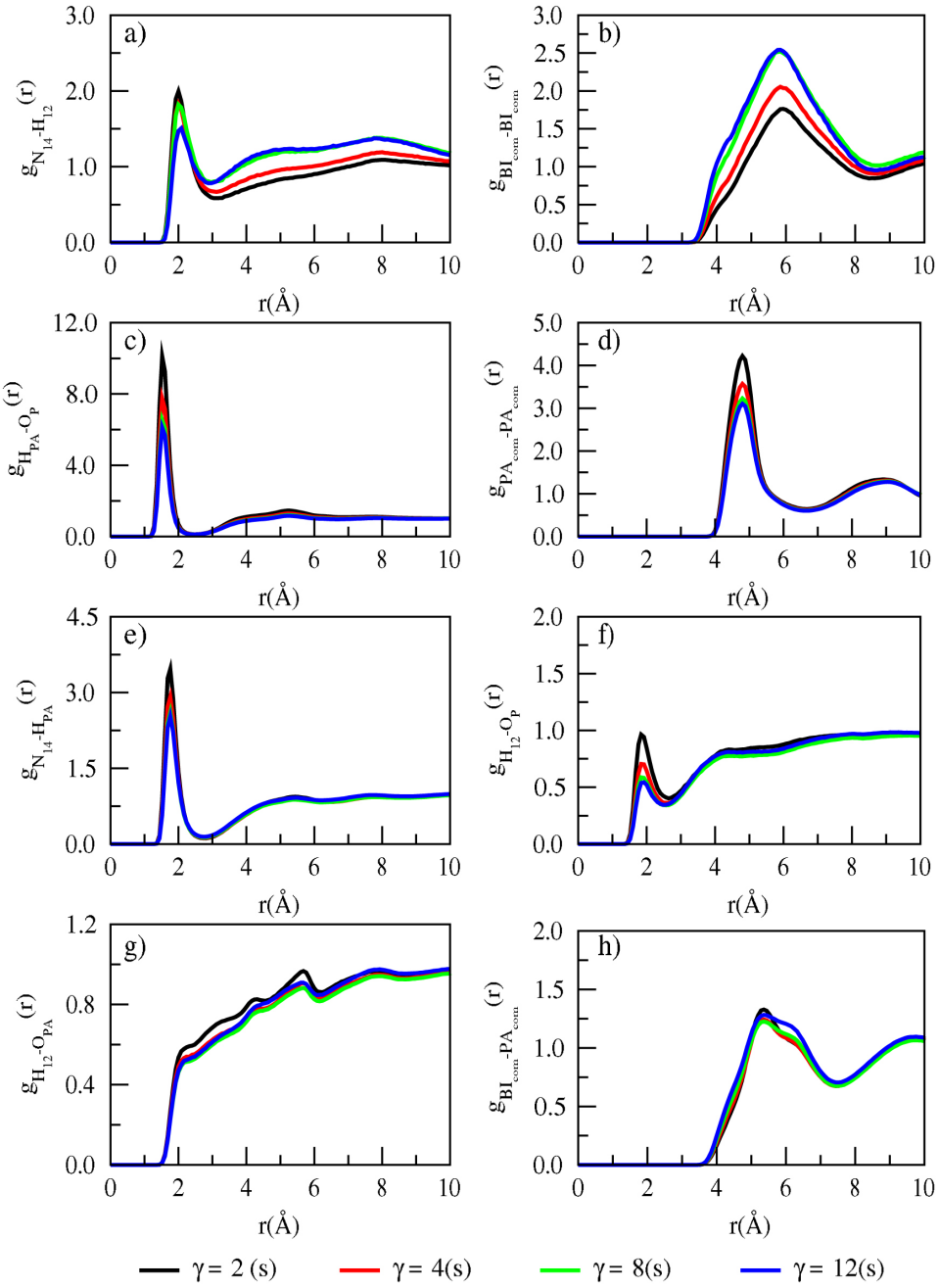

Figure 2.6: RDFs of PA doped BI mixtures at 450 K for a) N_{14}-H_{12}, b) BI_{com}-BI_{com}, c) H_{PA}-O_P, d) PA_{com}-PA_{com}, e) N_{14}-H_{PA}, f) H_{12}-O_P, g) H_{12}-O_{PA}, and h) BI_{com}-PA_{com}.

(γ = 12), which shows that increasing γ results in large solvation shells that are rich in PA molecules. The N_{14}–H_{PA} RDFs in Figure 2.6e show a first minimum at 2.5 Å. The first

peak position in the N_{14}–H_{PA} RDFs appears at 1.75 Å. The coordination number at the first minimum increases from 1.05 (γ = 2) to 1.5 (γ = 12). The increase in coordination number with γ occurs because the H_{PA} hydrogen is acidic in nature and prefers to orient around the imine nitrogen (N_{14}). An interaction between the amine hydrogen (H_{12}) of BI and the double-bonded nonprotonated oxygen (O_P) of PA can be discerned by examining the H_{12}–O_P RDFs shown in Figure 2.6f. The decrease in coordination number (obtained at the first minimum at 2.5 Å) with increasing γ demonstrates the poor ability of the amine hydrogen to participate in hydrogen bonding with the nonprotonated oxygen (O_P) of PA. The RDFs between the amine hydrogen (H_{12}) and the protonated oxygen (O_{PA}) are shown in Figure 2.6g. Unlike the other RDFs, the H_{12}–O_{PA} RDFs do not show a sharp minimum. However, a small shoulder is seen at 2.2 Å, which was chosen as the cutoff when calculating the coordination number at each γ. The coordination number increases from 0.34 (γ = 2) to 0.50 (γ = 12). An examination of the coordination numbers obtained from the H_{12}–O_{PA} and H_{12}–O_P RDFs in Table 2.3, shows that the strength of the interaction of the amine hydrogen (H_{12}) with the protonated oxygen atom (O_{PA}) increases with increasing γ, whereas there is a decrease in the interaction strength with the nonprotonated oxygen (O_P). The coordination numbers also offer indirect evidence that at large values of γ, the Grotthuss mechanism for proton transfer in PA-doped BI mixtures is more likely to occur via hydrogen bonding between the protonated oxygen (O_{PA}) of PA and the amine hydrogen (H_{12}) of BI (although this needs to be confirmed by ab initio MD simulations). The solvation of BI by PA molecules can be seen in the BI_{com}–PA_{com} RDFs shown in Figure 2.6h. Similar to the trends seen for the PA_{com}–PA_{com} RDFs, the coordination number increases from 3.50 (γ = 2) to 13.75 (γ = 12).

Table 2.3: Coordination numbers calculated at the first minimum at 450 K

γ	N_{14}-H_{12}	BI_{com}-BI_{com}	H_{PA}-O_P	PA_{com}-PA_{com}	N_{14}-H_{PA}	H_{12}-O_P	H_{12}-O_{PA}	BI_{com}-PA_{com}
2	0.30	7.75	0.60	8.15	1.05	0.64	0.34	3.50
4	0.19	5.90	0.70	10.20	1.30	0.25	0.36	9.75
8	0.10	4.40	0.71	11.20	1.42	0.20	0.38	12.50
12	0.05	2.80	0.75	12.50	1.50	0.19	0.50	13.75
Neat BI	1.10	12.50	-	-	-	-	-	-
Neat PA	-	-	0.79	13.13	-	-	-	-

2.3.4 Influence of PA uptake and temperature on diffusion

The diffusion coefficients calculated from the MSDs (see Figure B2-2 of the Appendix B) are shown in Table 2.4. For example, the diffusion of BI in PA-doped BI mixtures at 450 K was slower by a factor ranging from 14.83 (γ = 2) to 23.47 (γ = 12) compared to the diffusion of neat BI. However, the diffusion of PA in PA-doped BI mixtures at 450 K differed from that of neat PA by much smaller factors: 1.18 (γ = 2) to 1.04 (γ = 12). This shows that the diffusion of BI in PA-doped BI mixtures is significantly slower than the diffusion of neat BI, because the BI molecules can be trapped in the strong hydrogen-bonded network formed by the PA molecules. This observation is consistent with the RDFs (Figure 2.6e), which show that there is significant hydrogen bonding between the hydrogen (H_{PA}) of PA and the imine nitrogen (N_{14}) of BI. Further, the vehicular diffusion of PA barely changes as the amount of PA increases. Similar trends in the diffusion coefficients of BI and PA in PA-doped BI mixtures with various PA-doping levels were also observed at 350 K and 400 K. The effects of temperature on the diffusion are as

Table 2.4: Diffusion coefficients ($\times 10^{-7}$ cm^2 s^{-1}) obtained for BI and PA in replicated PA-doped BI mixtures based on the solvated configuration

γ	T (K)	BI	PA
2	350	0.20 ± 0.04	0.09 ± 0.01
	400	1.74 ± 0.18	1.00 ± 0.01
	450	9.29 ± 0.67	5.37 ± 0.13
4	350	0.11 ± 0.01	0.08 ± 0.00
	400	1.18 ± 0.18	0.96 ± 0.01
	450	7.40 ± 0.51	5.74 ± 0.03
8	350	0.13 ± 0.03	0.11 ± 0.00
	400	1.27 ± 0.01	1.35 ± 0.01
	450	6.21 ± 0.27	6.10 ± 0.33
12	350	0.16 ± 0.04	0.14 ± 0.01
	400	1.27 ± 0.08	1.42 ± 0.01
	400	5.87 ± 0.23	6.10 ± 0.02

follows. The diffusion of BI in PA-doped BI mixtures increases by a factor of $\sim$9 (γ = 2) from 350 K to 450 K. Similarly, the diffusion of PA in PA-doped BI mixtures increases by factor of $\sim$6 (γ = 2) from 350 K to 450 K. Indeed, increases in the diffusion coefficient with temperature are seen for all γ. For each temperature, the diffusion of BI decreases as γ increases, whereas the diffusion of PA increases.

2.3.5 Influence of PA uptake on the hydrogen-bond dynamics

Characterizing the formation and scission of hydrogen bonds (HBs) is a useful way to gain an understanding of proton transport mechanisms. Since classical force fields do not allow

bond breaking or formation, the focus is solely on the uninterrupted HB dynamics, which can be captured in the following manner: The HB dynamics are much faster than the self-diffusion of each type of molecule; hence, if a HB is broken, the same molecule could remain in the vicinity for some time before the same bond is reformed. A distribution of lifetimes, *h(t)*, is computed by a histogram of the HB number from *0* to *t*. The HB lifetime is calculated using the autocorrelation function, *C(t)*,[77,78] where,

$$C(t) = \frac{\langle h(0)|h(t)\rangle}{\langle h(0)|h(0)\rangle} \tag{2.1}$$

h(t)=1 if a pair is found to be linked by a hydrogen bond at time *t*, and 0 otherwise. The integral of *C(t)* gives an estimate for the average HB lifetime, τ_{HB}:

$$\tau_{\mathrm{HB}} = \int_O^\infty C(t)dt \tag{2.2}$$

Similar to the work of Spoel et al.,[79] the HB analysis performed in this work was realized in the following manner. The final snapshots of the various PA doped BI mixtures from a 20 ns production run at 450 K were chosen as input, and a short 250 ps production run was performed where the trajectories were recorded every 50 fs. The hydrogen bond probability distribution was calculated, where the length of the HB was considered to be the distance between the donor and acceptor atoms that participate in the hydrogen bonding[80–82] (see Figure B2-3 of the Appendix B), while the HB angle was considered to be the angle donor–hydrogen–acceptor (see Figure B2-4 of the Appendix B). The maximum cutoff distance and angle applied when calculating the HB dynamics (for each interaction and γ) were chosen based on Figures B2-3 and B2-4 respectively. For each interaction and γ, the HB number was normalized with respect to the number of PA molecules. Additionally, the HB number for the H_{12}–O_{PA} interaction was normalized with respect to the number of O_{PA} sites. The HB number and correlation times [C(t)] corresponding to the

HB interactions are shown in Figure 2.7. The HB number for N_{14}–H_{12} decreases, that for

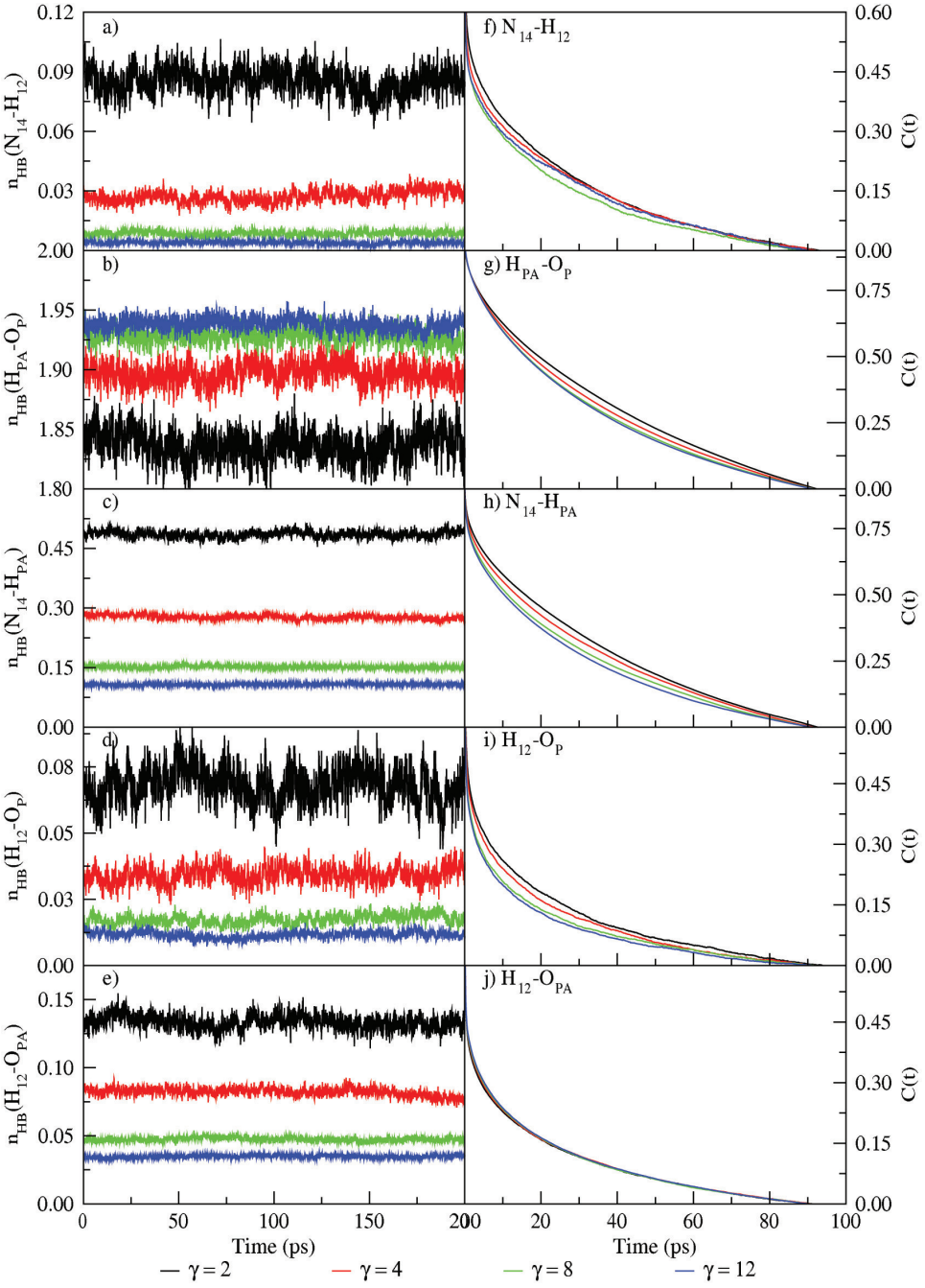

Figure 2.7: HB numbers a-e) and lifetimes f-j) of PA-doped BI mixtures at 450 K.

H_{PA}–O_P increases, that for N_{14}– H_{PA} decreases, that for H_{12}–O_P decreases, and that for

H_{12}–O_{PA} decreases with γ. The HB lifetimes are shown in Table 2.5. The HB lifetimes for H_{PA}–O_P, N_{14}–H_{PA}, and H_{12}–O_P decrease with γ. The HB lifetime for the H_{12}–O_{PA} interaction increases with γ. However, a corresponding decrease in the HB lifetime of H_{12}–O_P with γ is observed, and this is due to the competition between the HBs N_{14}–H_{12} and H_{12}–O_{PA}. The increase in the HB lifetime of the H_{12}–O_{PA} bond with increasing γ, in contrast to the decrease in the HB lifetime of the H_{12}–O_P bond, illustrates the strength of the interaction of the amine hydrogen (H_{12}) with the protonated oxygen (O_{PA}) as opposed to that with the nonprotonated oxygen (O_P) of PA. The MD simulations suggest that both BI and PA can act as proton acceptors and proton donors. However, such conclusions need to be confirmed by ab initio molecular dynamics (AIMD), which can show the actual process of proton transfer, including the formation and scission of hydrogen bonds and this is the focus of future activities.

Table 2.5: HB lifetimes (in ps) from a 250 ps production run

γ	N_{14}-H_{12}	H_{PA}-O_P	N_{14}-H_{PA}	H_{12}-O_P	H_{12}-O_{PA}
2	13.21	27.11	24.60	10.32	9.01
4	12.62	25.59	23.08	9.30	9.18
8	11.08	24.47	21.31	8.19	9.15
12	12.07	24.10	20.17	7.61	9.29

2.4 Conclusions

The structural and dynamical properties of neat BI, neat PA, and PA-doped BI mixtures were characterized by MD simulations. Different choices for the input configurations of the PA-doped BI mixtures resulted in similar structural and dynamical properties. The

RDFs showed that temperature has only a limited effect on the structural changes in the neat BI, neat PA, and PA-doped BI mixtures. The RDFs for the PA-doped BI mixtures show the presence of a strong hydrogen bond between the imine nitrogen N_{14} of BI and the hydrogen (H_{PA}) of PA where the imine nitrogen accepts the hydrogen from PA, which is further confirmed by HB analysis. The coordination numbers (Table 2.3) and HB lifetimes (Table 2.5) show that with increasing PA uptake, the interaction between the amine hydrogen (H_{12}) of BI and the protonated oxygen (O_{PA}) of PA increases in strength, whereas the interaction between the amine hydrogen (H_{12}) of BI and the nonprotonated oxygen (O_P) of PA decreases. The diffusion of BI decreases with increasing PA uptake. In the next chapter, the interactions of phosphoric acid with ABPBI is examined. The effect of polymer chain length and temperature on structure and dynamics is investigated.

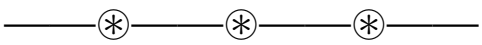

Chapter 3

Effect of polymer chain length and temperature on structure and dynamics of phosphoric acid doped ABPBI [poly(2,5-benzimidazole)] polymer electrolyte membrane

3.1 Introduction

In the preceding chapter, the interactions between BI and PA at various PA concentrations were characterized, where these properties provided an excellent benchmark. However, an inclusion of a polymeric form of BI is required to mimic the properties of macromolecular system which can validate existing experimental studies. Sunda et al.[83] employed MD simulations and observed that the degree of hydration showed a significant influence on structure and dynamics in various hydrated environments of PA doped ABPBI membrane. The authors observed that the number of PA molecules around the ABPBI polymer chain decrease significantly with hydration, and an inclusion of trifluoromethanesulfonic acid results in a decrease in water mobility. The effect of PA doping and temperature have not been examined in non-humidified PA doped ABPBI membrane. The hetero-

aromatic nature of the polymer membrane which increases with polymer chain length can influence the structural properties of the polymer membrane. The objective of this chapter is to characterize the effect of polymer chain length, PA doping and temperature on various structural and dynamical properties of PA doped ABPBI membrane. In order to demonstrate the effect of polymer chain length; dimer, trimer, tetramer, pentamer and decamer units of the ABPBI membrane were chosen. Sunda et al.[83] demonstrated that an increasing polymer chain length from decamer to icosamer results in negligible effect on structure and dynamics of hydrated PA doped ABPBI membrane. Based on their observations and to simulate a large polymeric system, simulations on a hectamer was performed and compared with the structural and dynamical properties obtained from a decamer. The input preparation of polymers of varying chain lengths with various PA doping, force-field parameters and details of MD simulations are described in Section 3.2. The structure and dynamical properties calculated from MD simulations are presented in Section 3.3. A summary of key findings concludes this chapter.

3.2 Computational details

The chemical structure of ABPBI membrane ["n" is a repeat unit of the membrane used for generation of polymers of varying chain length or Molecular Weight (MW)] and PA, with atom types (used for description of structural properties) is shown in Figure 3.1. MD simulations were performed using the GROMACS[61] 4.5.4 program. The force-field parameters of the ABPBI membrane were taken from the OPLS-AA force-field database.[84] Force-field parameters of PA were extracted from the work of Spieser et al.[63] The input configurations of a dimer (n = 2, MW = 234), trimer (n = 3, MW = 350), tetramer (n = 4, MW = 466), pentamer (n = 5, MW = 582), decamer (n = 10, MW = 1163) and hectamer (n = 100, MW = 11602) was generated using a molecular builder program.

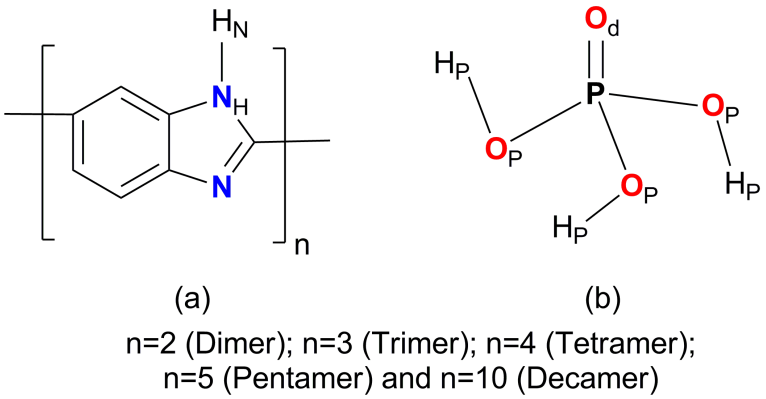

Figure 3.1: Chemical structures with atom types of a) ABPBI polymer membrane and b) phosphoric acid (PA).

Each configuration (dimer, trimer, tetramer, pentamer and decamer) was energy-minim ized using the steepest descent algorithm.[58] The energy minimized configuration was replicated in three directions of a cubic box to create a large system containing N = 128 polymer replicas. In order to obtain a density close to an experimental density, a simulated annealing was performed on the replicated systems in the following manner: each system was heated from 300 K to 1000 K and cooled back to 300 K with an annealing time of 1.35 ns. The annealing procedure was repeated five times for a total annealing time of 6.75 ns and the final configuration used as an input for a 10 ns equilibration (isobaric-isothermal: NPT) at T = 300 K, 350 K, 400 K and 450 K. The calculated density (from the last 5 ns equilibration) of a decamer is (1.35 g cm^{-3} , T = 300 K) is in good agreement with the experimental[85] density (1.4 g cm^{-3}, T = 298 K). The final configuration obtained from this equilibration was chosen as a template to create configurations which vary in amount of PA doping. The amount of PA doping chosen is γ = 1.6, 3.0 and 3.7, where, γ denotes the number of PA molecules per monomer unit of ABPBI membrane. The choice of γ was based on the experimental work of Kim et al.[32] and Asensio et al.[31,33,35] on PA doped ABPBI membrane. Further, the neutral form of PA is included in this work due to the following reasons: a) The Infrared spectroscopy measurements of Glipa et al.[86] on PA doped

PBI membranes show that the neutral form of PA is in equilibrium with its corresponding ionic species,[87] and b) the limitations of the classical force-field used in this work do not permit the dissociation of PA into phosphate ions. Nevertheless, the inclusion of neutral PA can offer a molecular level understanding of the interactions in neutral PA and with the polymer membrane.

For configuration (dimer, trimer, tetramer, pentamer and decamer) which contains 128 polymer replicas and various PA doping (γ = 1.6, 3.0 and 3.7), MD simulations were performed at T = 300 K, 350 K, 400 K and 450 K. The cut-off for calculation of van der Waals and electrostatic interactions was chosen as 12 Å. The Particle-Mesh Ewald[66,67] method was used for calculation of long-range electrostatic interactions. The leapfrog algorithm[49] was used to integrate the equations of motion with a time-step of 1 fs. Each system was equilibrated for 10 ns using the NPT ensemble at a constant 1 bar isotropic pressure maintained by a Berendsen barostat.[64] The velocity-rescale thermostat[65] was chosen to keep the systems set at the target temperature. The number of PA molecules (calculated based on each polymer chain and γ), total number of atoms in the system and cubic box length is shown in Table 3.1. The instantaneous densities are shown in Figure B3-1 of the Appendix B.

The calculated densities from the last 5 ns of the equilibration run are shown in Table 3.2. As seen, density increases with polymer chain length. At 300 K and γ = 1.6, the density calculated for a dimer is 1.56 g cm^{-3}, tetramer is 1.60 g cm^{-3} and pentamer is 1.61 g cm^{-3}. Similar trends in density are also seen at γ = 3.0 and γ = 3.7, and T = 350 K, 400 K and 450 K. The final configuration from the equilibration run was chosen as an input for a 10 ns production run using the isochoric-isothermal (NVT) ensemble. A final snapshot from the production run in PA doped ABPBI membrane is shown in Figure B3-2 of the Appendix B. Trajectories from the production run were recorded every 5 ps for calculation of various structural and dynamical properties. The results presented in Sections

Table 3.1: The number of PA molecules, total number of atoms and cubic box length (after equilibration)

Polymer chain length	PA doping (γ)	Number of PA molecules	Total Number of atoms	Box Length (Å)	
				300 K	450 K
Dimer (n = 2)	1.6	410	6864	42.040	42.606
	3.0	768	9728	47.153	47.974
	3.7	947	11160	49.432	50.162
Trimer (n = 3)	1.6	614	10160	47.979	48.429
	3.0	1152	14464	53.742	54.540
	3.7	1421	16616	56.363	57.157
Tetramer (n = 4)	1.6	819	13464	52.534	53.200
	3.0	1536	19200	59.106	59.895
	3.7	1894	22064	61.905	62.839
Pentamer (n = 5)	1.6	1024	16768	56.415	57.194
	3.0	1920	23936	63.629	64.451
	3.7	2368	27520	66.686	67.584
Decamer (n = 10)	1.6	2048	33280	71.316	71.739
	3.0	3840	47616	80.506	81.118
	3.7	4736	54784	84.038	84.998

3.3.1 – 3.3.6 are from ABPBI polymer membrane constructed from Dimer to Decamer in a single chain.

In order to investigate the differences in structural and dynamical properties between

Table 3.2: Density (ρ) obtained from a 5 ns equilibration run

Polymer chain length	PA doping (γ)	ρ (g cm^{-3})			
		300 K	350 K	400 K	450 K
Dimer (n = 2)	1.6	1.56	1.55	1.53	1.50
	3.0	1.66	1.64	1.62	1.58
	3.7	1.68	1.66	1.64	1.61
Trimer (n = 3)	1.6	1.59	1.58	1.56	1.53
	3.0	1.67	1.66	1.64	1.61
	3.7	1.71	1.68	1.66	1.63
Tetramer (n = 4)	1.6	1.60	1.59	1.57	1.54
	3.0	1.69	1.67	1.64	1.61
	3.7	1.72	1.69	1.66	1.64
Pentamer (n = 5)	1.6	1.61	1.60	1.58	1.55
	3.0	1.69	1.67	1.65	1.61
	3.7	1.72	1.69	1.67	1.64
Decamer (n = 10)	1.6	1.59	1.59	1.58	1.57
	3.0	1.67	1.66	1.65	1.63
	3.7	1.71	1.70	1.68	1.65

a Decamer and polymer chain lengths larger than the Decamer (and to simulate a large polymeric system), Hectamer (n = 100) of the ABPBI polymer membrane was chosen. The input configuration of the Hectamer was created (constructed from 100 monomer units with a total of 1302 atoms in each chain), energy minimized and replicated in a

cubic box to contain 16 polymer replicas. The replicated configuration was used as input for a simulated annealing procedure as described earlier. The final configuration from the annealing procedure was solvated with 2560 PA molecules (γ = 1.6). After energy minimization, the PA doped configuration was pre-equilibrated for 1 ns using the NPT ensemble, followed by a 10 ns NPT equilibration (at 300 K and 450 K). Equilibration was followed by a 20 ns production run using the NVT ensemble. Section 3.3.7 describes the structural and dynamical properties (calculated from the trajectories of the production run) of Hectamer and its comparison with a Decamer (γ = 1.6 and T = 300 K and 450 K).

3.3 Results and Discussion

3.3.1 Intra and Inter chain membrane interactions

The interactions in the polymer membrane can be seen from an examination of N-N, N-N_H and N-H_N RDFs (Figure 3.2 and Figure B3-3 of Appendix B) and coordination numbers calculated at γ = 1.6, 3.0 and 3.7 (Figure 3.2). All coordination numbers are calculated at the first minima of the RDFs. For each polymer chain length and PA doping, a first and second peak from the N-N RDFs (Figure 3.2a, Figure B3-3a,b) appears at 4.8 Å and 6.1 Å which correspond to inter-chain and intra-chain interactions respectively. The peak positions resemble closely with work of Sunda et al.[83] on hydrated PA doped ABPBI membrane. This suggests that exclusion of hydration does not impact the interactions in the membrane. The first peak of the N-N_H RDFs at 3 Å (Figure 3.2c, Figure B3-3c,d) shows inter-chain interactions, whereas intra-chain interactions are seen only at 6.1 Å, with a small peak at 5.2 Å (inset of Figure 3.2c and Figure B3-3c,d) absent in a Decamer. The peak of N-H_N RDFs at 5.2 Å and 6.1 Å correspond to a separation of N-H_N by six and seven bonds respectively.[83] In a dimer, the intensity of N-H_N intra-chain inter-

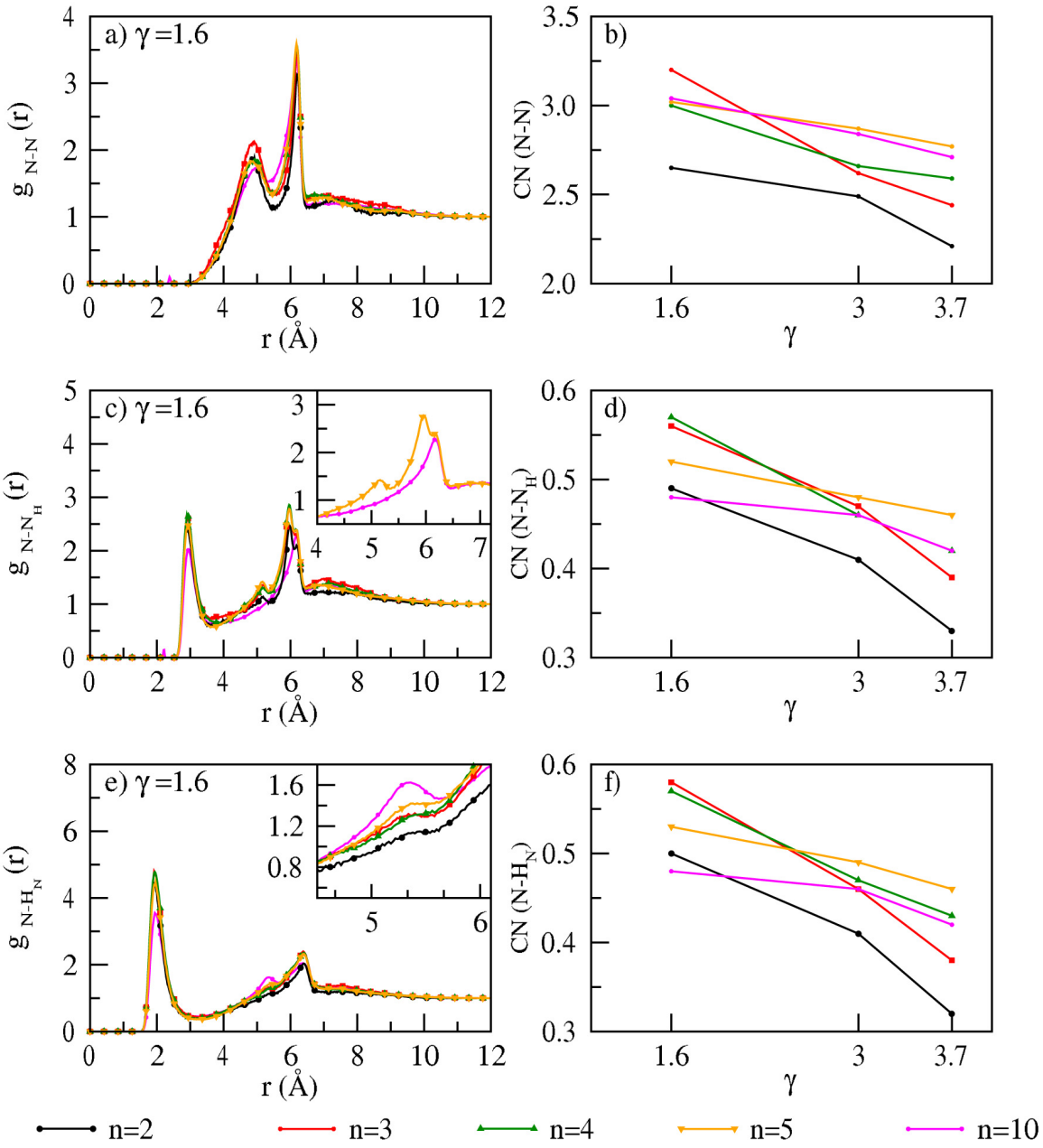

Figure 3.2: RDFs (γ = 1.6) and coordination numbers (for all PA doping) of (a and b) N-N, (c and d) N-N_H and (e and f) N-H_N interactions at T = 300 K.

actions at 5.2 Å is very low and increases with polymer chain length (inset of Figure 3.2e, Figure B3-3e,f). The increase in intensity could be due to increasing possibility of free rotation around the C-C single bond which connect adjacent benzimidazole moieties. The

coordination numbers from the N-N, N-N_H and N-H_N RDFs decrease with increase in PA doping. This is because more amount of PA can interact with the membrane matrix thereby reducing the interactions within the membrane. Further, a negligible effect of temperature on RDF profiles and coordination numbers is observed which illustrates the thermal stability of the membrane.

3.3.2 Phosphoric Acid and Membrane-Phosphoric Acid interactions

The various interactions in PA are seen from RDFs (Figure 3.3 and Figure B3-4 of Appendix B) and coordination numbers calculated at γ = 1.6, 3.0 and 3.7 (Figure 3.3). The variation in polymer chain length has no effect on all interactions. The interactions between PA molecules show the following features: The P-P RDFs show a first minimum at 6 Å, higher than the minimum at 5.5 Å reported on hydrated[83] PA doped ABPBI membrane. This shows that unlike membrane interactions (as discussed in Section 3.3.1), the solvation shell of PA is different in hydrated and dry environments. As expected, the coordination numbers from the P-P RDFs shows (see Figure 3.3b) an increase with PA doping. The coordination numbers show that the interaction between the non-protonated oxygen atom (O_d) and hydrogen atoms (H_P) of PA show (see Figure 3.3d) a slight increase with PA doping. This shows that the double bonded oxygen atom has less preference for hydrogen bonding with other PA molecules.

The membrane-phosphoric acid interactions elucidated from the coordination numbers show the following features: The interaction between the nitrogen atom (lone pair) of the benzimidazole moiety of the membrane and the hydrogen atom of PA (H_P) shows an increase with PA doping (see Figure 3.3f). This compensates the decreasing interactions seen within the membrane with increasing PA doping. The hydrogen bond interactions between the hydrogen atom of the imidazole moiety (H_N) and the double bonded oxygen atom of PA (O_d) slightly increases with PA doping (see Figure 3.3h). This again shows that

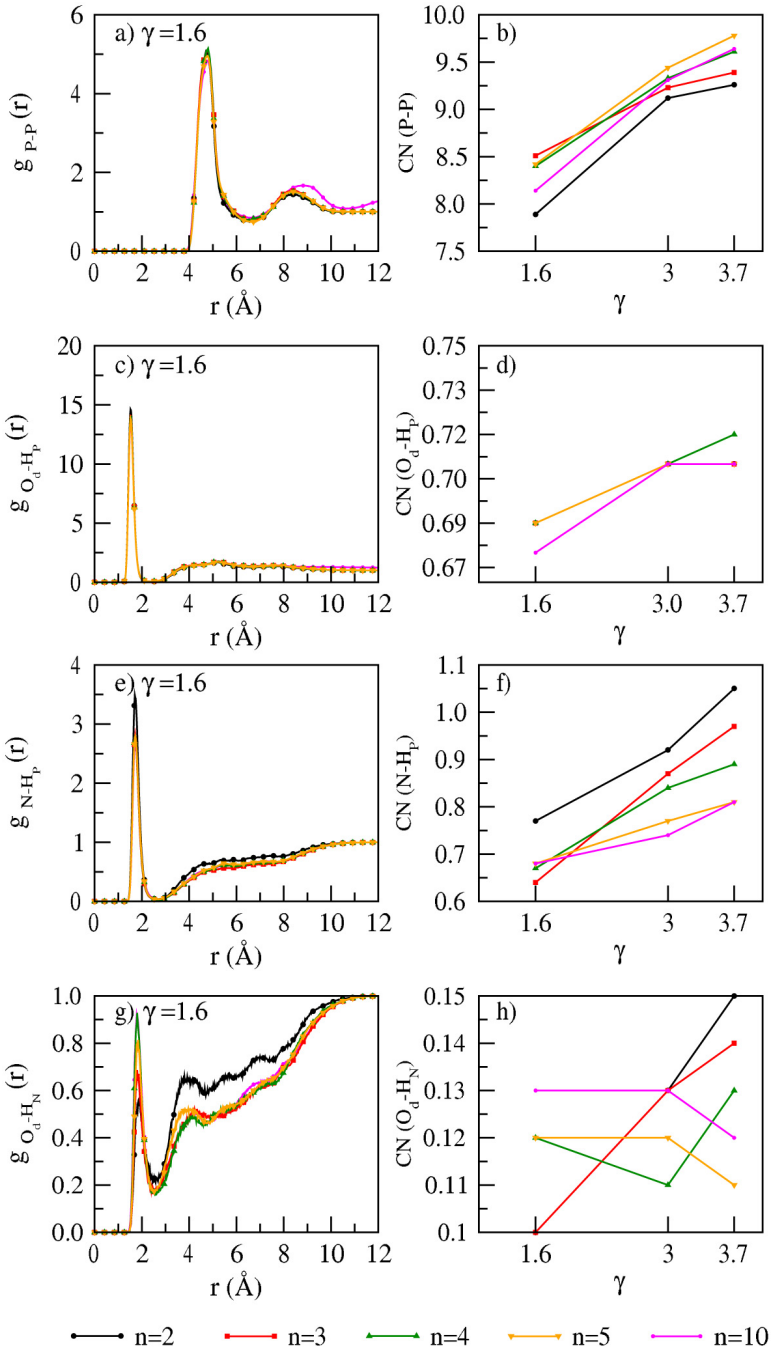

Figure 3.3: RDFs (γ = 1.6) and coordination numbers (for all PA doping) of (a and b) P-P, (c and d) O_d-H_P, (e and f) N-H_P and (g and h) O_d-H_N interactions at T = 300 K.

the double bonded oxygen atom has less preference for interactions with the membrane. The variation in temperature shows no effect on RDF profiles and coordination numbers.

3.3.3 Radius of gyration and end-to-end distance

The radius of gyration, R_g, for each polymer chain is calculated using Eqn. 1.10 where, M_i is the mass of atom i, r_i is the position of atom i with respect to the center of mass of the ABPBI polymer chain. This is further illustrated by a normalized probability distribution plot of a "**time averaged**" radius of gyration ($\langle R_g \rangle_t$) and end-to-end distance ($\langle R_{E\text{-}E} \rangle_t$) calculated for N = 128 polymer replicas at γ = 1.6 (see Figure 3.4). The normalized

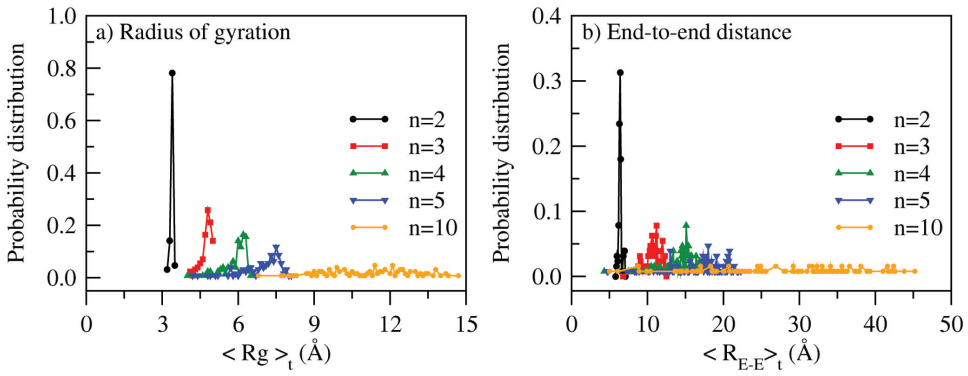

Figure 3.4: Normalized probability distribution (for N = 128 polymer replicas) for various polymer chain length (n = 2, 3, 4, 5, 10) at γ = 1.6 using (a) time averaged radius of gyration ($\langle R_g \rangle_t$) and (b) time averaged end-to-end distance ($\langle R_{E\text{-}E} \rangle_t$).

.

probability plot shows a broad distribution of $\langle R_g \rangle_t$ and $\langle R_{E\text{-}E} \rangle_t$ which increases with polymer chain length (from n = 2 to n = 10). For example, in the case of Dimer, a sharp peak of Gaussian probability distribution is observed which diminishes in the Decamer. Similar trends are seen at γ = 3.0 and γ = 3.7.

For each polymer chain length, PA doping and temperature, a "**time and system (N = 128) averaged**" radius of gyration ($\overline{R}_g$) and the end-to-end distance ($\overline{R}_{E\text{-}E}$) is calculated. The effect of polymer chain length, PA doping and temperature on $\overline{R}_g$ and $\overline{R}_{E\text{-}E}$ shows the following trends: At 300 K, $\overline{R}_g$ increases linearly with polymer chain length for all PA doping (Figure 3.5a). Similar trends are seen at other temperatures. For each polymer chain length and temperature, the increase in PA doping shows no effect on $\overline{R}_g$.

For each polymer chain length and PA doping, the effect of temperature on $\overline{R}_g$ is insignificant (Figure 3.5b). Similar to the trends seen in $\overline{R}_g$, $\overline{R}_{E\text{-}E}$ remains invariant to change in PA doping and temperature. $\overline{R}_{E\text{-}E}$ increases linearly from a Dimer to Tetramer (Figure 3.6), though a deviation in linearity is seen in a Pentamer and Decamer. A deviation in linearity of $\overline{R}_{E\text{-}E}$ in a Pentamer and Decamer can be attributed to the flexibility of the membrane which arises from more unrestricted rotations around the C-C bond with an absence of aromatic ring current drive through the single bond which connects benzimidazole segments. Asensio et al.[31] used thermal gravimetric analysis on PA doped ABPBI membrane and concluded that the glass transition temperature (T_g) of ABPBI is higher than the membrane degradation temperature (560 °C).[88] Hence, calculated $\overline{R}_g$ and $\overline{R}_{E\text{-}E}$ suggest the stability of the membrane within the temperature range.

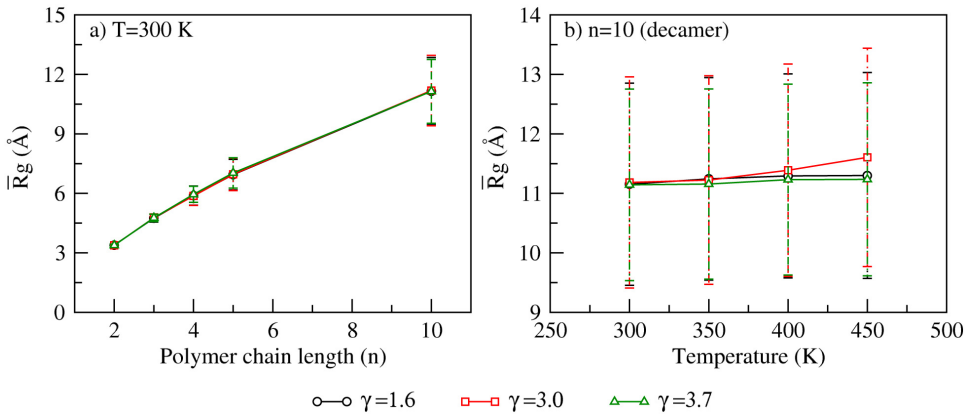

Figure 3.5: Time and system averaged radius of gyration ($\overline{R}_g$) calculated at varying PA doping for (a) various polymer chain length (n = 2, 3, 4, 5, 10) at T = 300 K and (b) decamer (n = 10) at different temperatures. (Error bars are standard deviation of $\overline{R}_g$).

The error bar in Figure 3.5 and Figure 3.6 represents standard deviation of $\overline{R}_g$ or $\overline{R}_{E\text{-}E}$. For all PA doping and temperature, the standard deviation in $\overline{R}_g$ and $\overline{R}_{E\text{-}E}$ increases with polymer chain length. This trend is consistent with the broadening of probability distribution with increasing polymer chain length (see Figure 3.4). The effect of PA doping on $\overline{R}_g$ and $\overline{R}_{E\text{-}E}$ is examined by a calculation of scaling exponents (υ)[89–91] at 300 K and 450

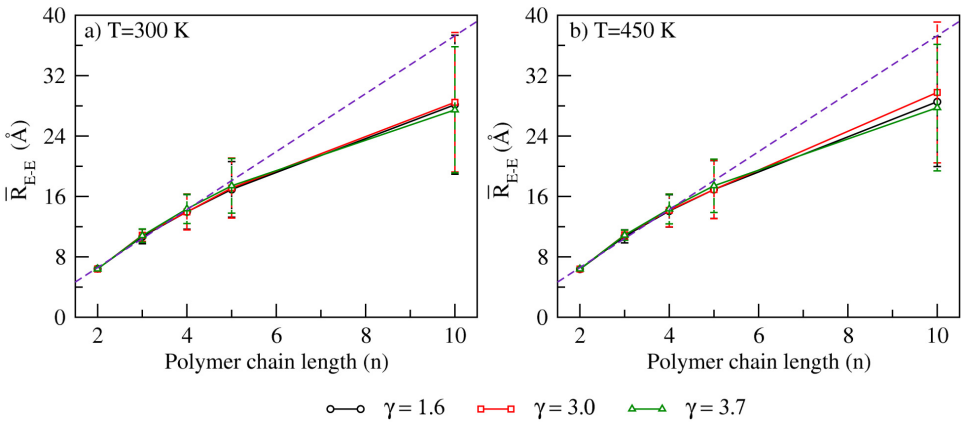

Figure 3.6: Time and system averaged end-to-end distance ($\overline{R}_{\text{E-E}}$) at varying PA doping for various polymer chain length (n = 2, 3, 4, 5, 10) at (a) T = 300 K and at (b) T = 450 K respectively. (Error bars are standard deviation of $\overline{R}_{\text{E-E}}$).

K. The scaling exponent can be expressed as:

$$R = cn^{\upsilon} \tag{3.1}$$

where, R is either $\overline{R}_{\text{g}}$ or $\overline{R}_{\text{E-E}}$, c is a constant and n is "chain length". The variation of $\overline{R}_{\text{g}}$ and $\overline{R}_{\text{E-E}}$ with polymer chain length (n = 2, 3, 4, 5 and 10) is fitted using equation 3.1. For all γ, the calculated υ at 300 K and 450 K are shown in Table 3.3. The υ value for $\overline{R}_{\text{g}}$ is 0.73, which closely resembles a characteristic polymer chain behavior (υ = 0.75)[92] where Self-Avoiding Walks (SAWs) of ABPBI polymer chains in PA are two-dimensional.[89–92] The υ value for $\overline{R}_{\text{E-E}}$ is 0.9, which represents the SAWs of ABPBI polymer chains in PA are confined to one dimension. In conclusion, the effect of PA doping and temperature on scaling exponents is insignificant. The calculations shows that the behavior of ABPBI membrane differ from the work of Wang et al.[93,94] on polyethylene terephthalate oligomers where authors found the υ value of 0.59 to represent a three dimensional SAWs of polymer chains. A higher υ value in ABPBI membrane could be due to the compact packing of polymer chains in a highly dense PA environment.

Table 3.3: Scaling exponent (υ) calculated for radius of gyration ($\overline{R}_{\mathrm{g}}$) and end-to-end chain ($\overline{R}_{\mathrm{E\text{-}E}}$) distance at 300 and 400 K

PA doping(γ)	υ from $\overline{R}_g$		υ from $\overline{R}_{E-E}$	
	300 K	450 K	300 K	450 K
1.6	0.736	0.746	0.902	0.913
3.0	0.738	0.760	0.908	0.934
3.7	0.737	0.743	0.889	0.895

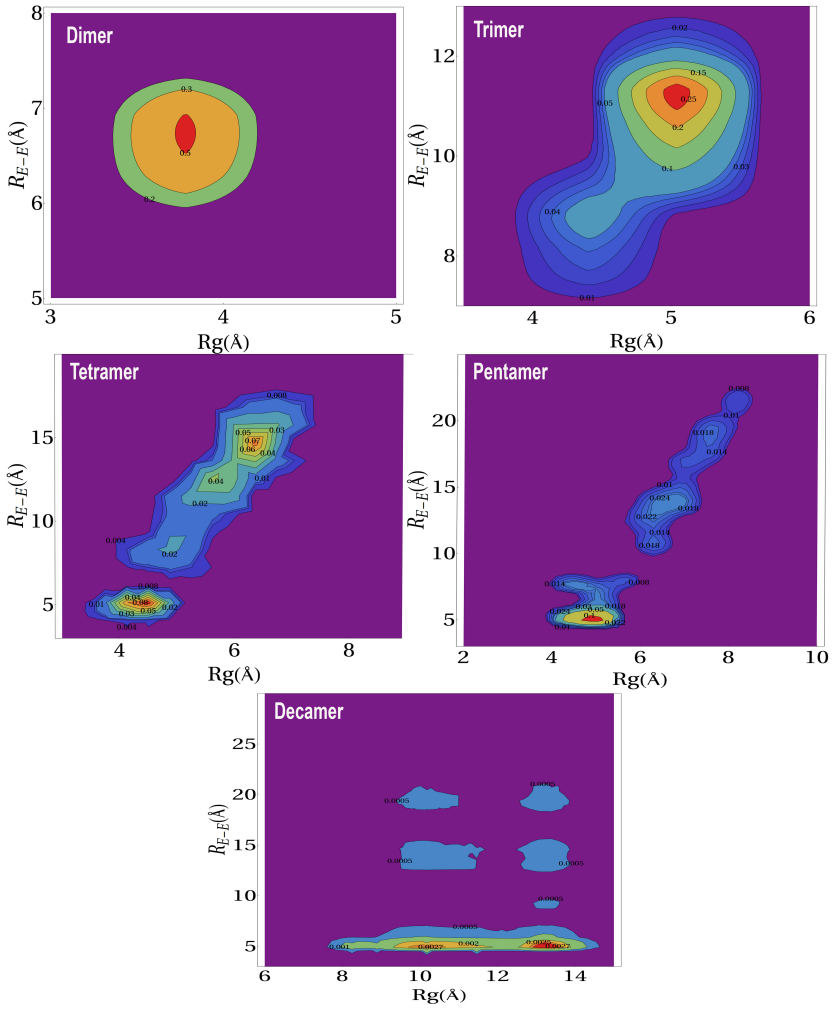

Figure 3.7: R_g vs R_{E-E} at γ = 1.6 and T = 300 K.

An examination of R_g vs R_{E-E} in Fig 3.7 shows the following features: In a dimer, a large number of configuration have 3.3 Å $\leq R_g \leq$ 4.3 Å and 6 Å $\leq R_{E-E} \leq$ 7 Å. With increasing chain length (trimer to decamer) there is spread of configurations especially towards higher R_g and R_{E-E}. In the case of a decamer, the configurations exist over a large range of values of R_g suggesting the existence of highly skewed and extended polymer chain lengths.

3.3.4 Cluster analysis

a. Interactions between benzimidazole moiety: A visual[57] inspection of polymer chain (Dimer to Decamer) with the lowest R_g (skewed) and the highest R_g (extended) is shown in Figure 3.8. To obtain further insights into inter-chain interactions and orientations of benzimidazole (BI) units, only a skewed polymer chain as a reference polymer chain is chosen to characterize the interactions of other polymer chains around this reference polymer chain. To illustrate this, a cluster analysis is performed using the Gromos algorithm[95] with a 12 Å distance (the cutoff used in MD simulations for non-bonding interactions) at γ = 1.6 and 300 K. The Gromos clustering method is based on the Root Mean Square Displacement (RMSD) of the structure. To find the clusters in the given trajectory, first RMSD is calculated over the trajectory then for each structure the numbers of the other structures whose RMSD is within 0.1 nm or less was calculated. The structure with highest number of neighbors is taken as center of cluster, and together with all neighboring structure forms the first cluster. A snapshot of polymer chains (of various R_g) around the skewed configuration of a Dimer, Trimer, Tetramer and Pentamer, respectively is shown in Figure 3.9. Inter-chain interactions with respect to the center of mass of each BI unit of a skewed polymer chain with other polymer chains from the BI_{com}-BI_{com} RDFs is examined. The details of calculation of the BI_{com}-BI_{com} RDFs are shown in Figure B3-5 (see Appendix B). For each polymer chain length, a peak at 5.2 Å (Figure 3.9) seen from the

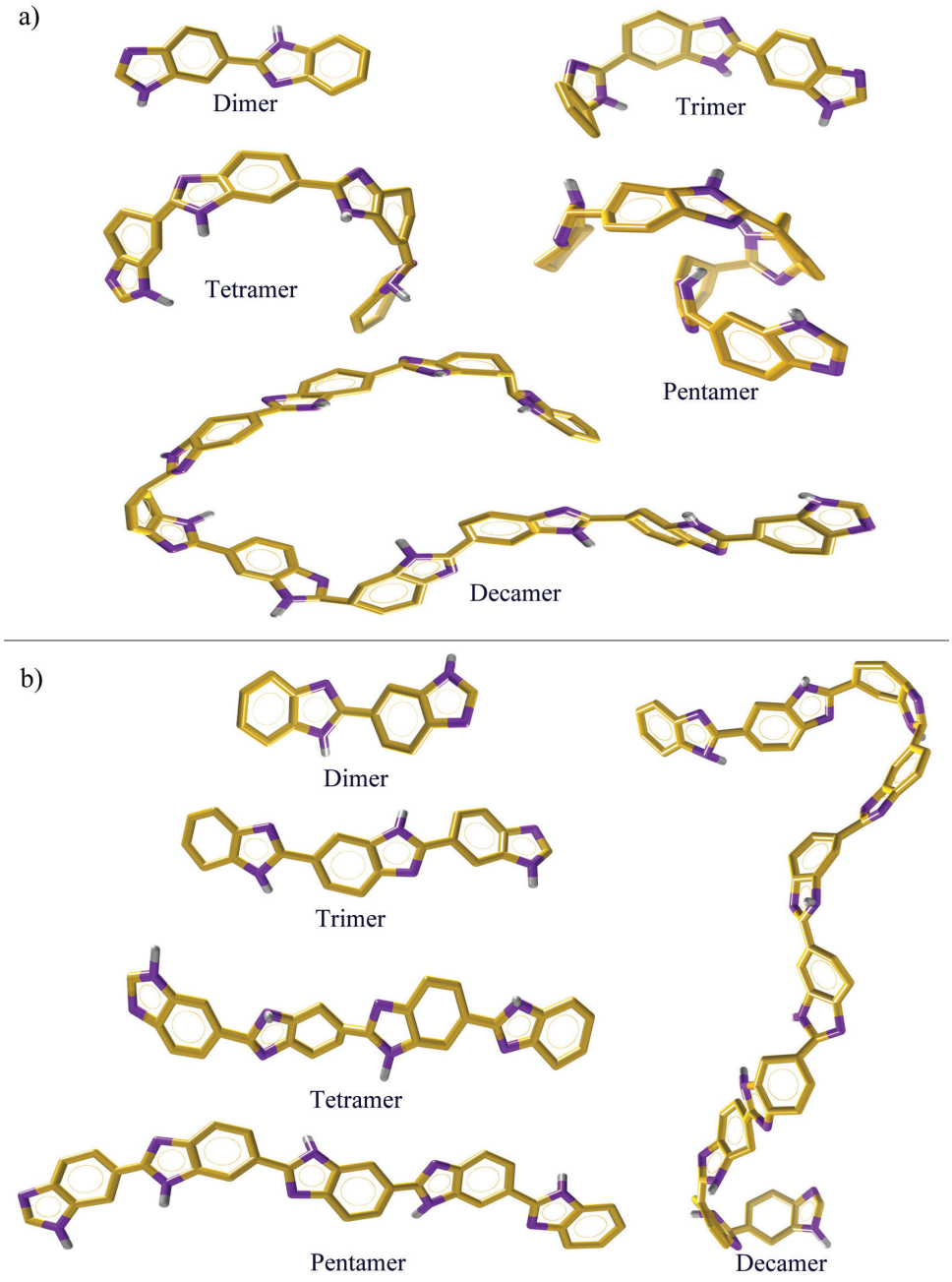

Figure 3.8: Snapshots of (a) skewed and (b) extended ABPBI membrane for various polymer chain length [benzimidazole ring: orange, hydrogen: grey, nitrogen: violet (Licorice)] at 300 K.

BI_{com}-BI_{com} RDFs show that the inter-chain BI distance (center of mass to center of mass) is higher than the geometrical criteria[96] (3.4 to 3.8 Å) of π-π interaction. Hence, the peak

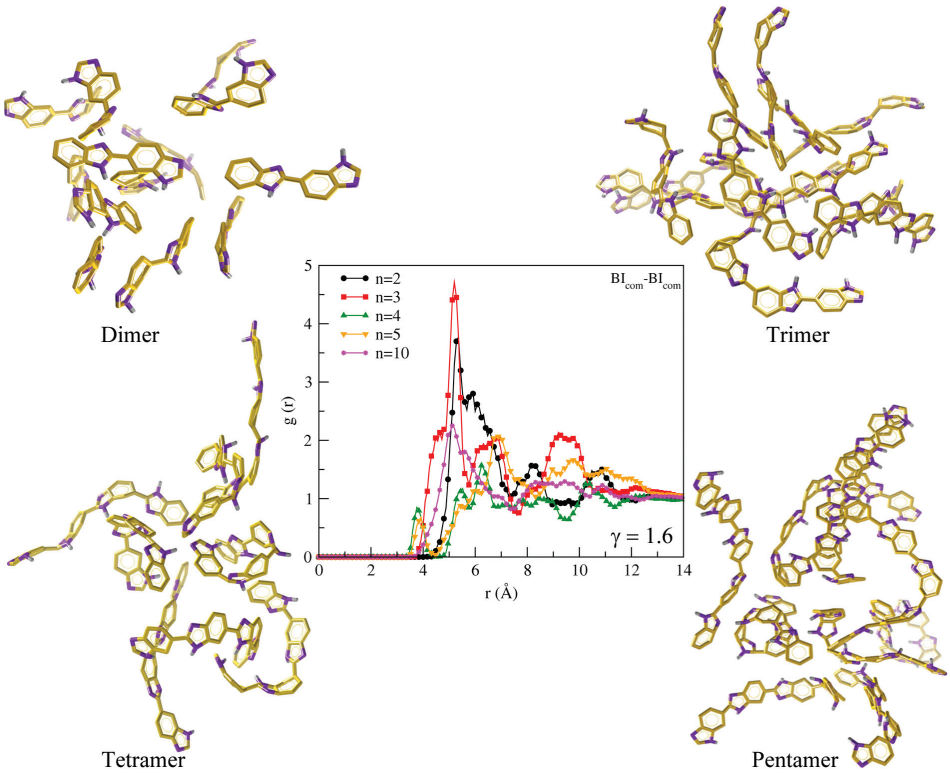

Figure 3.9: Snapshots of ABPBI polymer chain clusters for dimer (top left), trimer (top right), tetramer (bottom left), pentamer (bottom right) and RDF's (at γ = 1.6) for center of mass to center of mass of any benzimidazole unit in ABPBI cluster (center) at 300 K [benzimidazole ring: orange, hydrogen:grey, nitrogen: violet (Licorice)].

distance from the BI_{com}-BI_{com} RDFs suggest that the nearest distance between any two inter-chain BI moiety can be only from N-N_H inter-chain interactions which appears at a distance of 3 Å (see Figure 3.2). Additionally, a low intensity peak from the BI_{com}-BI_{com} RDFs appears at ∼4.2 Å in a tetramer and pentamer. The presence of low intensity peaks could arise from van der Waals interactions or C-H/π interactions[97–99] of aromatic ring in BI moieties which is difficult to distinguish from an all atom simulation performed in the this work.

b. PA clusters around the polymer chain: For each polymer chain length, PA doping and temperature, a skewed and an extended polymer configuration to calculate the number

of PA molecules present in a cluster calculated using the criteria described earlier were chosen. The average number of PA molecules around the skewed and extended polymer chain at 300 K and 450 K is shown in Figure 3.10. The number of PA molecules in

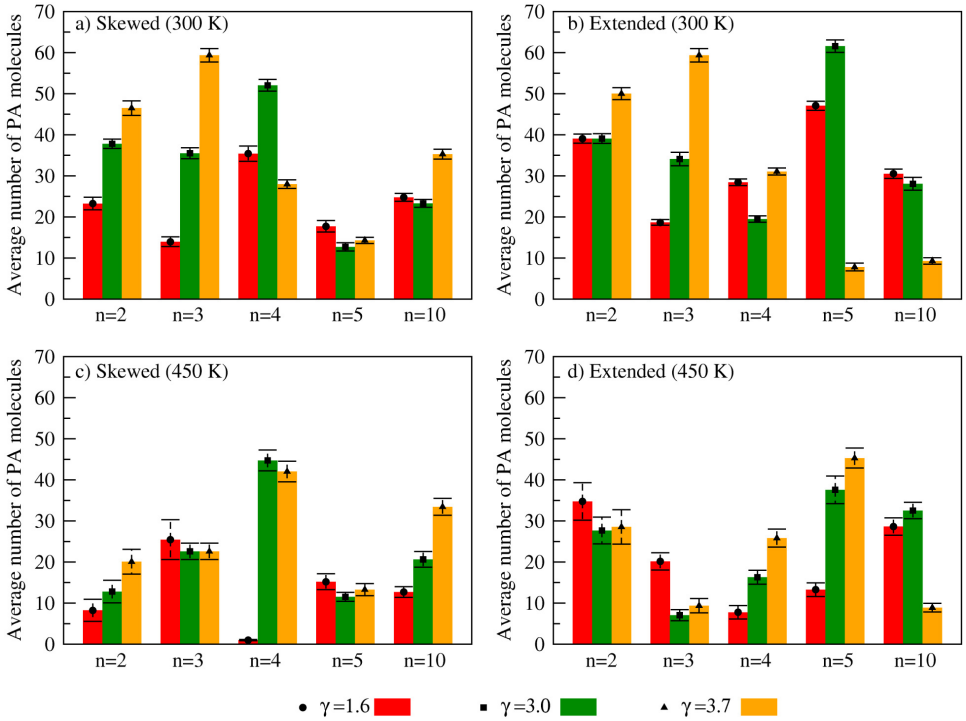

Figure 3.10: Average number of PA molecules in a cluster around the skewed and extended ABPBI membrane at (a and b) T = 300 K and (c and d) T = 450 K.

a cluster shows no particular trend with variation in polymer chain length and PA doping. However, a significant effect of temperature is seen on the average number of PA molecules which forms a cluster. For example, compared to 300 K, a decrease of ∼25-30% in the number of PA molecules at 450 K is observed around the skewed or extended configuration with varying polymer chain length and PA doping.

3.3.5 Diffusion of PA

The MSDs calculated using Eqn. 1.8 are shown in Figure B3-6 of Appendix B. The diffusion coefficients (shown in Figure 3.11) of PA calculated from the linear regime (2 ns-8

ns) with the corresponding values is shown in Table A3-1 (See Appendix A). The effect of

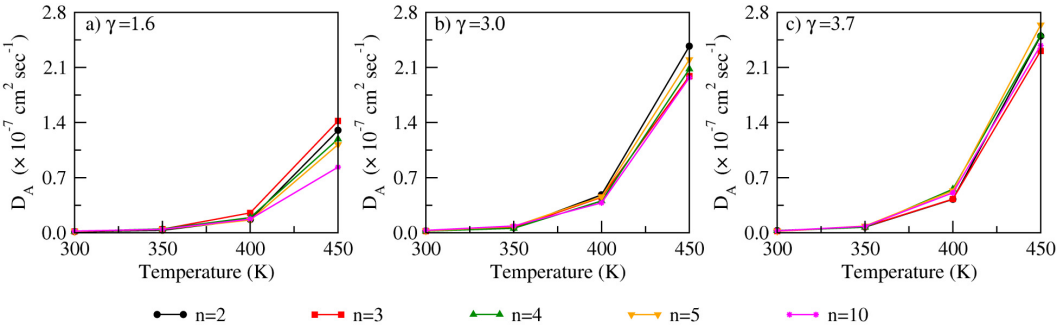

Figure 3.11: Diffusion coefficient (D_A) of PA using varying polymer chain length (n = 2, 3, 4, 5, 10) at (a) γ = 1.6, (b) γ = 3.0 and (c) γ = 3.7.

polymer chain length on the diffusion coefficient of PA is insignificant, though diffusion coefficients are slightly lower in a Decamer compared to Dimer only at 450 K. For each polymer chain length and temperature, a significant effect of PA doping is seen on the diffusion coefficient of PA. For example, in a Decamer, at 450 K, the diffusion coefficient of PA increase by a factor of ∼2.3 from γ = 1.6 to γ = 3.0. An increase from γ = 3.0 to γ = 3.7, results in an increase in the diffusion coefficient of PA by a factor of ∼1.2. For each polymer chain length and PA doping, an increase in temperature results in a significant increase in PA mobility. For e. g., in a Decamer, at γ = 3.0, the diffusion coefficient of PA increases by a factor of ∼2.8 from 300 K to 350 K. Further, increase in temperature from 350 K to 400 K and 400 K to 450 K results in increase in diffusion coefficient of PA by a factor of ∼4.3 and ∼5.2, respectively.

3.3.6 Activation energy of diffusion

The calculated diffusion coefficients of PA at 300 K, 350 K, 400 K and 450 K are used to calculate the activation energy of diffusion (E_A) of PA (see Eqn. 1.9) where, E_A is calculated from the slope of linear fit. The calculated E_A values are presented in Table 3.4. The variation in PA doping gives similarity in E_A of PA at low polymer chain length

Table 3.4: Activation energy of diffusion (E_A) from a 10 ns production run

Polymer chain length	PA doping(γ)	Activation energy(E_A)
Dimer (n = 2)	1.6	33.29
	3.0	35.25
	3.7	33.45
Trimer (n = 3)	1.6	32.74
	3.0	34.13
	3.7	35.06
Tetramer (n = 4)	1.6	31.14
	3.0	34.42
	3.7	34.51
Pentamer (n = 5)	1.6	30.08
	3.0	33.41
	3.7	36.17
Decamer (n = 10)	1.6	26.99
	3.0	30.63
	3.7	34.25

(Dimer and Trimer). For example, the E_A of PA for Dimer is 33.29 kJ mol^{-1} (γ = 1.6) and 33.45 kJ mol^{-1} (γ = 3.7), and in Trimer is 32.74 kJ mol^{-1} (γ = 1.6) and 35.06 kJ mol^{-1} (γ = 3.7). The E_A of PA in Decamer is 26.99 kJ mol-1 (γ = 1.6), 30.63 kJ mol^{-1} (γ = 3.0) and 34.25 kJ mol^{-1} (γ = 3.7) respectively. These trends in calculated E_A values are in qualitatively agreement with the experiment E_A of PA [27.4 kJ mol^{-1} (γ = 2.7) and 39.8 kJ mol^{-1} (γ = 3.0)] reported by Asensio et al.[33] The difference in E_A calculated from the work is due to the presence of water molecules in the experimental work of Asensio et al.[33]

3.3.7 Effect of long polymer chain length on structure and dynamics

The influence of long polymer chain length is examined by a comparison of structural and dynamical properties obtained from a Decamer and Hectamer. As seen (Table A3-2 of Appendix A), the densities obtained from MD simulations using a Decamer and Hectamer resemble very closely. An examination of N-N, N-N_H and N-H_N RDFs (Figure B3-7 of Appendix B) show that structural properties from a Decamer and Hectamer are similar. As

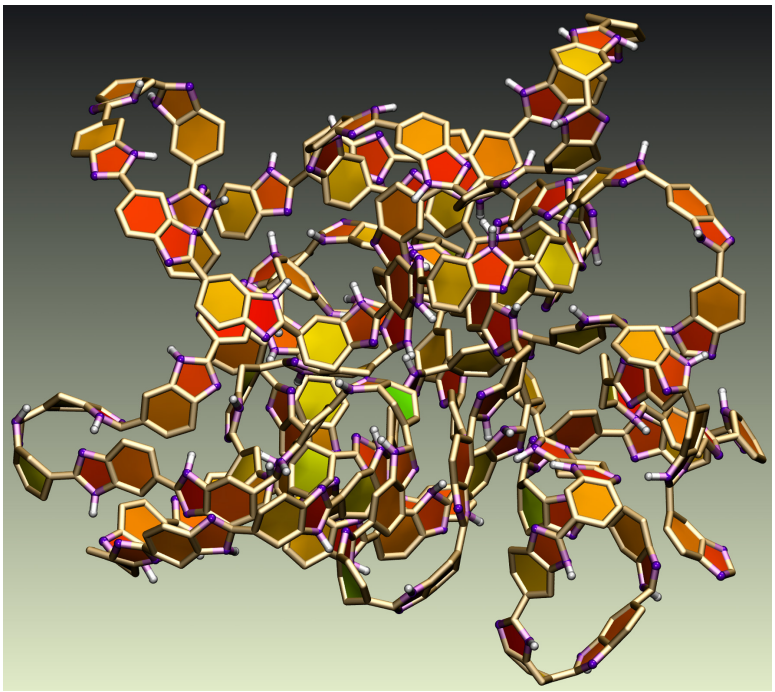

Figure 3.12: Snapshot of a single polymer chain of hectamer (n = 100) of ABPBI membrane (γ = 1.6) at 300 K [benzimidazole ring: paperchain; hydrogen: white (CPK); nitrogen: violet (CPK)].

expected, due to increasing chain length, the end-to-end polymer chain distance shows a difference between a Decamer and Hectamer. For e.g., the $\overline{R}_{\text{E-E}}$ is 28.15 Å for a Decamer and 48.66 Å for a Hectamer (see Table A3-2 of Appendix A). However, the radius of gyration shows a small change from a Decamer to Hectamer. For e. g., the $\overline{R}_{\text{g}}$ for Decamer is 11.15 Å and 14.91 Å for a Hectamer (γ = 1.6, T = 300 K). Similar trends are seen at

T = 450 K. The dynamical properties of PA obtained from the MSDs (Figure B3-8 of Appendix B) and diffusion coefficients (Table A3-2 of Appendix A) show similar behavior from a Decamer and Hectamer.

A representative snapshot of a Hectamer (extracted from the final snapshot of a production run) shown in Figure 3.12 illustrates enhanced coiling of polymer chain compared to the Decamer (see Figure 3.9). Nevertheless, the similarity in properties between Decamer and Hectamer does indicate that the Decamer can be an optimum chain length of ABPBI membrane.

3.3.8 Conclusions

A molecular investigation on structure and dynamics of PA doped ABPBI membrane is performed using varying polymer chain length, PA doping and temperature. An examination of properties calculated using polymer chain lengths from Dimer to Decamer shows the following trends: An increase in polymer chain length and PA doping show a more dense packing of polymer membrane, where the intra-chain hydrogen-bonding interaction (N-H_N) increase significantly with polymer chain length. The variation in temperature does not affect the N-N, N-N_H and N-H_N interactions between sites in the membrane, within sites in PA and between the membrane and PA. The variation in polymer chain length and temperature has insignificant effect on interactions in PA, whereas interactions increase with PA doping. The radius of gyration and end-to-end distance of various polymer chains remains unaffected with PA doping and temperature which show the thermal stability of the PA doped ABPBI membrane. A scaling exponent of 0.73 for $\overline{R}_g$ and 0.9 for $\overline{R}_{E\text{-}E}$ suggest that the inclusion of PA shows the Self-Avoiding Walk of ABPBI polymer chains in one or two dimensions.

The interactions and orientations of benzimidazole units seen from the BI_{com}-BI_{com} RDFs and BI-BI clusters shows that inter-chain benzimidazole interactions are from N-H_N

hydrogen bonding. The random orientations of BI units and the presence of free rotation around the single bond which connects two monomeric BI segments lead to minimal possibility of π-π interactions. The number of PA molecules in a cluster around the polymer chain is invariant to polymer chain length and PA doping, though increasing temperature leads to reduced number of PA molecules. The effect of PA doping and temperature shows a significant impact on diffusion of PA, but remains unchanged with variation in polymer chain length. The activation energy of PA diffusion is unaffected by polymer chain length at higher doping (γ = 3.0 or γ = 3.7). The structural and dynamical properties using a Decamer and Hectamer exhibit identical characteristics. A molecular understanding of effect of polymer chain length, PA doping and temperature effects can guide experimental efforts to deploy these membranes in fuel cell applications.

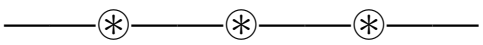

Chapter 4

Summary and outlook

4.1 Conclusions

The salient features of the thesis are as follows:

- Benzimidazole-based polymer membranes like poly(2,5-benzimidazole) (ABPBI) doped with phosphoric acid (PA) are electrolytes that exhibit high proton conductivity in fuel cells at elevated temperatures. The benzimidazole (BI) moiety is an important constituent of these membranes, so the present work was performed in order to achieve a molecular understanding of the BI–PA interactions in the presence of varying levels of the PA dopant, using classical MD simulations. The various hydrogen-bonding interactions, as characterized based on structural properties and hydrogen-bond lifetime calculations, show that both BI and PA molecules exhibit dual proton-acceptor/donor functionality. An examination of diffusion coefficients showed that the diffusion of BI decreases with increasing PA uptake, whereas the diffusion of PA slightly increases. The hydrogen-bond lifetime calculations pointed to the existence of competitive hydrogen bonding between various sites in BI and PA.

- The effect of polymer chain length using a dimer to hectamer have been investigated using MD simulation methods. Results from the simulations (dimer to decamer) show the following trends: the inter-chain and intra-chain interactions in membrane are unaffected with polymer chain length and temperature, though a

significant increase with PA doping is observed. The radius of gyration linearly increases with polymer chain length and remains unchanged with PA doping and temperature. However, the end-to-end distance deviates from linearity with polymer chain length which suggests increasing coiling of the membrane. The diffusion coefficient of PA increases with PA doping and temperature, but remains constant with polymer chain length. The activation energy of diffusion of PA decreases significantly with an increase in polymer chain length at low PA doping, but remains unaffected at higher PA doping. A comparison of the structural and dynamical properties of a decamer and a hectamer shows that the decamer represents the optimum polymer chain length beyond which no significant change in properties is observed.

4.2 Future directions

The use of PA as dopant for proton conduction in anhydrous conditions does possess challenges such as corrosion and leaching from membrane matrix leading to reduced fuel cell performance.[10,23–27] However, these issues can be addressed by use of Ionic Liquids (IL) as proton carriers.[100–102] IL exhibit properties such as low melting temperature, low vapor pressure, high ionic conductivity, high thermal stability and nonflammability.[103,104] Protic Ionic liquids (PILs) can be obtained by combining Bronsted acid and Bronsted base that transfer proton from acid to base thus making proton donor and acceptor sites to form a hydrogen bond network.[105] From several PILs investigated, Yasuda et al.[106] concluded that the N,N-diethyl-N-methylammonium triflate ([dema][TfO]) to be a suitable candidate for fuel cell application due to its low overpotential in fuel cell reactions. Nakamoto et al.[104] characterized the electrochemical properties of N,N-diethyl-N-methylammonium triflate ([dema][TfO]) under anhydrous conditions. Watanabe and co-workers[107,108] reported the use of [dema][TfO] as an electrolyte in H_2 fuel cell operating at 150°C with an increased

reaction rate at the electrodes and high ionic conductivity. Chang et al.[109] calculated the structural and dynamical properties of neat and hydrated [dema][TfO] using MD simulations and reported high ionic conductivity at T = 167 °C. Johnson et al.[110] studied the effect of temperature on electrode kinetics in [dema][TfO] based H_2 fuel cells. The authors reported increased electrode kinetics at higher operating temperature (>100 °C) under non-humidified conditions. Liu et al.[111] reported high thermal stability of ([dema][TfO] doped PBI membranes) and obtained an ionic conductivity upto 20.73 mS cm^{-1} (T = 160 °C). The authors concluded that Grotthuss[44] and vehicular diffusion contribute to proton conduction.

A focus of future activity is to examine interactions between [dema][TfO] and PBI membrane using MD simulations. The structure and dynamics at various thermodynamical conditions can be calculated. The actual mechanism of proton transfer can be seen from *ab initio* MD simulations such as BOMD[112] which is also one of the future directions. The calculated proton conductivity can be compared with experiments. Finally, several others ILs can be investigated as suitable dopants.

Appendix A

Table A2-1: Densities (g cm^{-3}) from a replicated solvated configuration.

Temperature (K)	γ = 2	γ = 4	γ = 8	γ = 12
350	1.477	1.600	1.693	1.732
400	1.452	1.573	1.665	1.703
450	1.417	1.540	1.633	1.672

Table A3-1: Diffusion coefficient (D_A) from a 10 ns production run.

Polymer chain length	PA doping (γ)	D_A of PA ($\times 10^{-7}$ cm^2 sec^{-1})			
		300 K	350 K	400 K	450 K
Dimer (n = 2)	1.6	0.0137	0.0314	0.1676	1.3010
	3.0	0.0222	0.0630	0.4812	2.3701
	3.7	0.0276	0.0714	0.4241	2.5001
Trimer (n = 3)	1.6	0.0171	0.0463	0.2520	1.4201
	3.0	0.0217	0.0648	0.4497	1.9901
	3.7	0.0205	0.0762	0.4276	2.3101
Tetramer (n = 4)	1.6	0.0164	0.0492	0.1927	1.1901
	3.0	0.0214	0.0564	0.4039	2.0810
	3.7	0.0266	0.0699	0.5532	2.5110
Pentamer (n = 5)	1.6	0.0174	0.0424	0.1614	1.1201
	3.0	0.0250	0.0807	0.4568	2.201
	3.7	0.0209	0.0847	0.5329	2.6401
Decamer (n = 10)	1.6	0.0212	0.0439	0.1741	0.8332
	3.0	0.0307	0.0865	0.3801	1.9701
	3.7	0.0247	0.0813	0.5073	2.381

Table A3-2: Average density (g cm^{-3}), end-to-end polymer chain distance ($\overline{R}_{\text{E-E}}$), radius of gyration ($\overline{R}_{\text{g}}$) and Diffusion coefficient (D_A ($\times 10^{-7}$ cm^2 sec^{-1})) of PA (γ = 1.6) in PA doped ABPBI membrane.

System Temperature	Decamer (n = 10)		Hectamer (n = 100)	
	300 K	450 K	300 K	450 K
Density (g cm^{-3})	1.59	1.57	1.62	1.57
$\overline{R}_{\text{E-E}}$(Å)	28.15 ±9.20	28.55 ±8.59	48.66 ±12.68	48.95 ±13.58
$\overline{R}_{\text{g}}$(Å)	11.15 ±1.69	11.30±1.72	14.91 ±0.89	15.11 ±0.85
D_A of PA	0.02 ±0.01	0.83 ±0.05	0.01 ±0.01	1.23 ±0.06

Appendix B

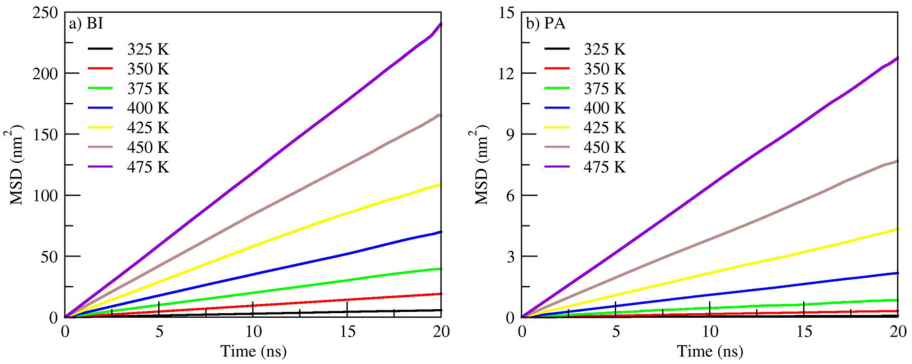

Figure B2-1: MSD of a) neat Benzimidazole and b) neat Phosphoric Acid.

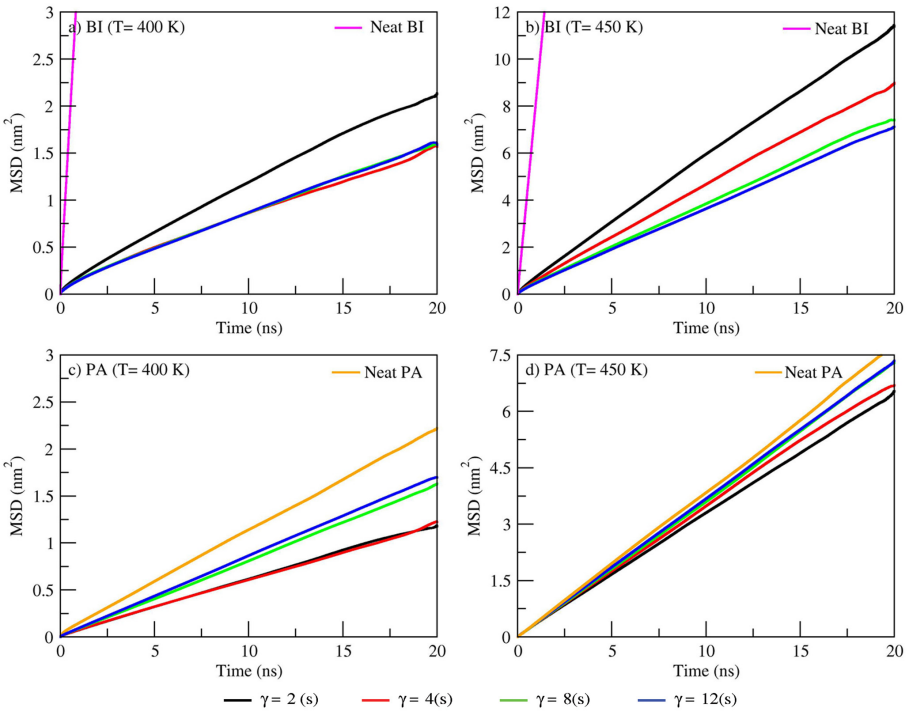

Figure B2-2: MSD of a) BI and b) PA in PA-doped BI mixtures at 400 K and 450 K.

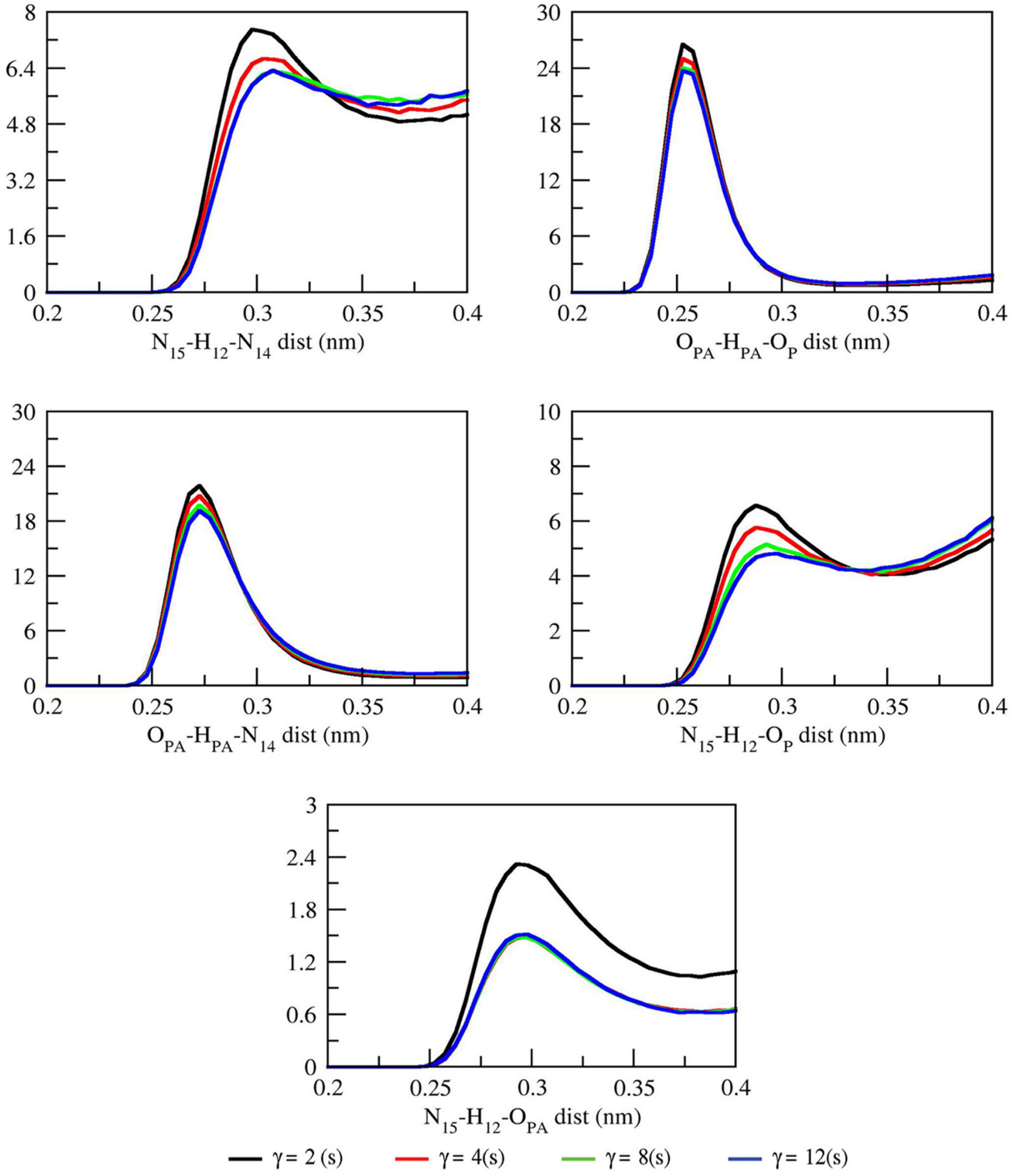

Figure B2-3: Hydrogen bond distribution vs. Donor-Hydrogen-Acceptor distance.

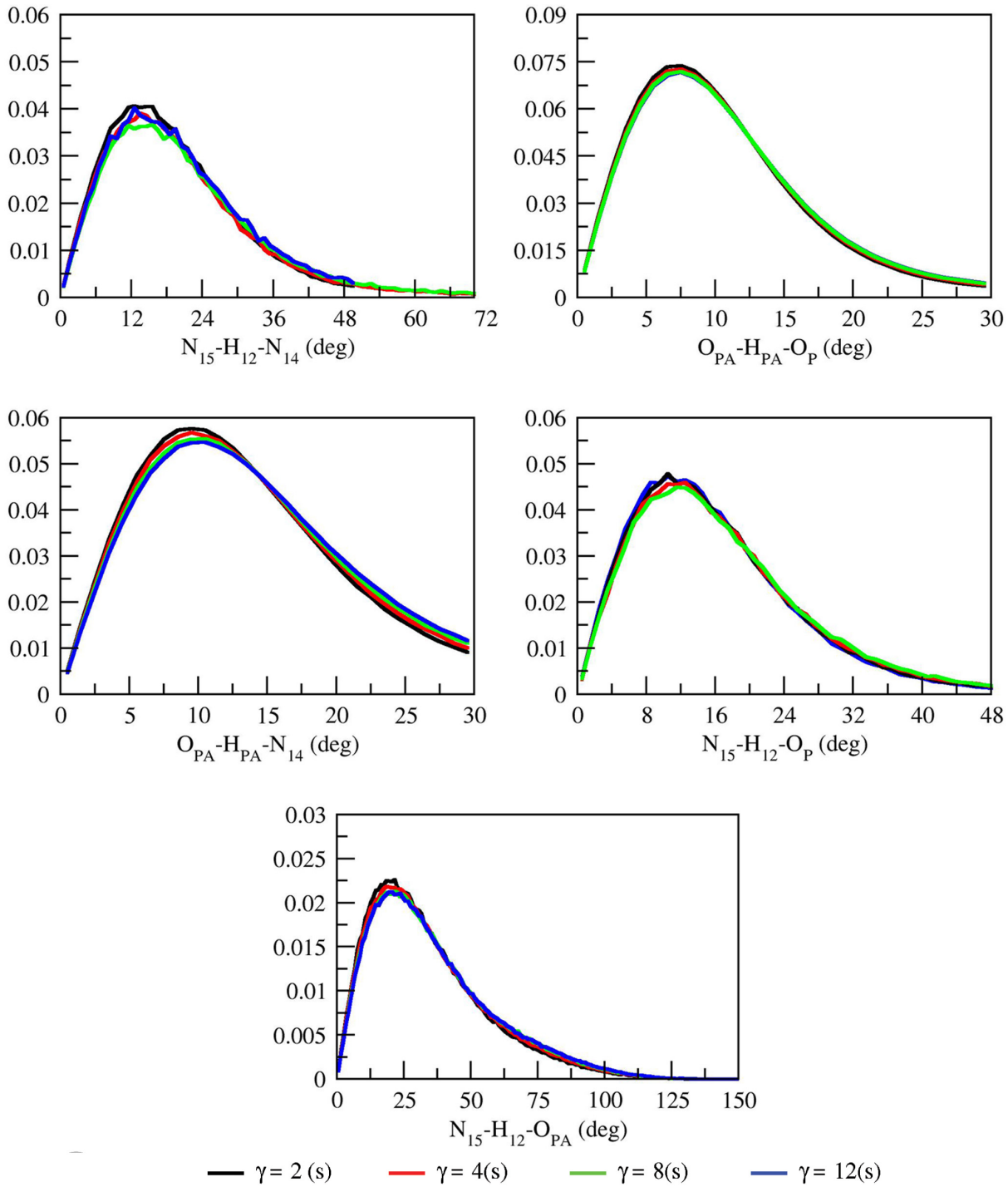

Figure B2-4: Hydrogen bond distribution vs. Donor-Hydrogen-Acceptor angle.

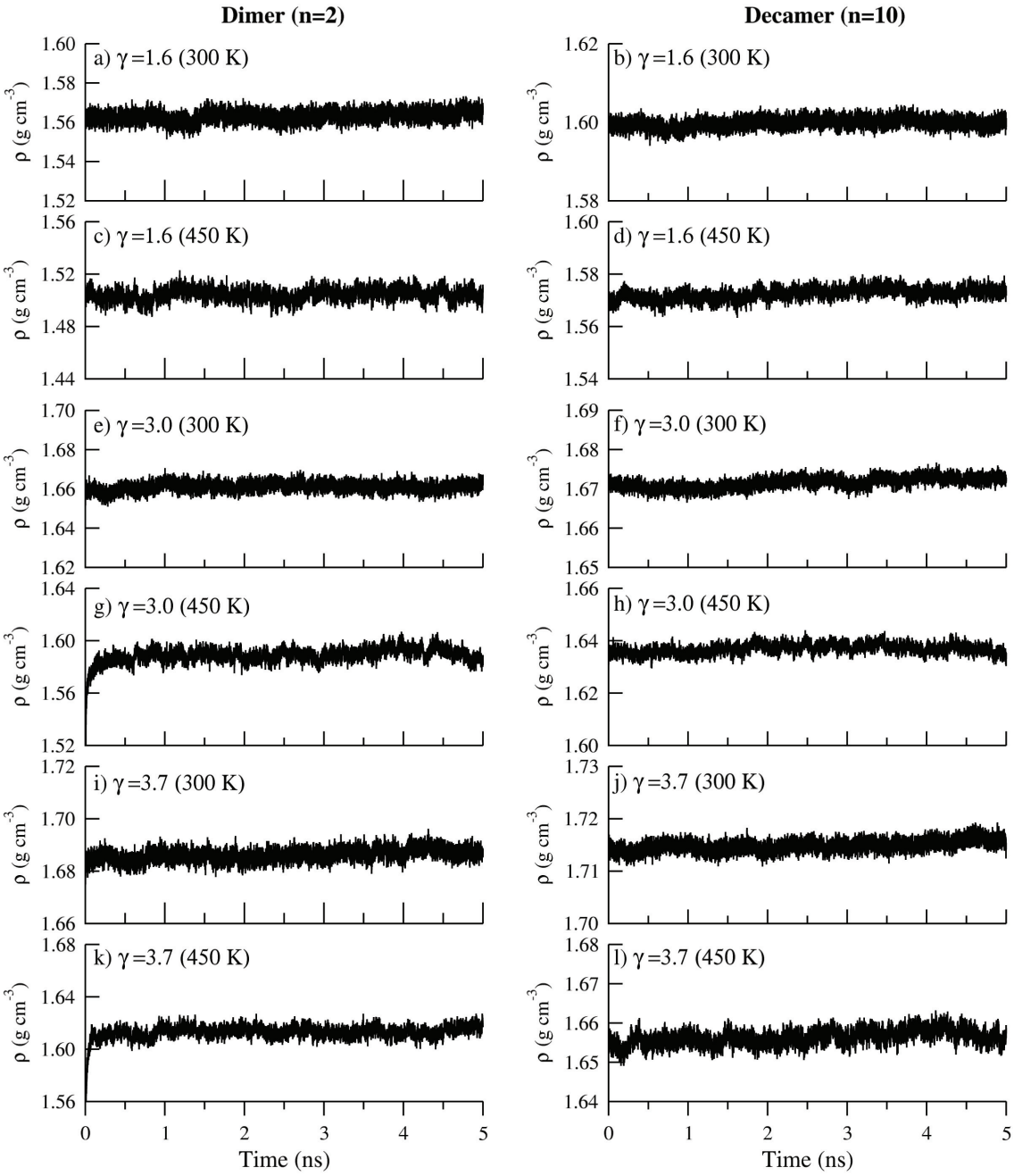

Figure B3-1: Density of PA doped ABPBI membrane for dimer and decamer from last 5 ns of equilibration at a-d) γ = 1.6, e-h) γ = 3.0 and i-l) γ = 3.7.

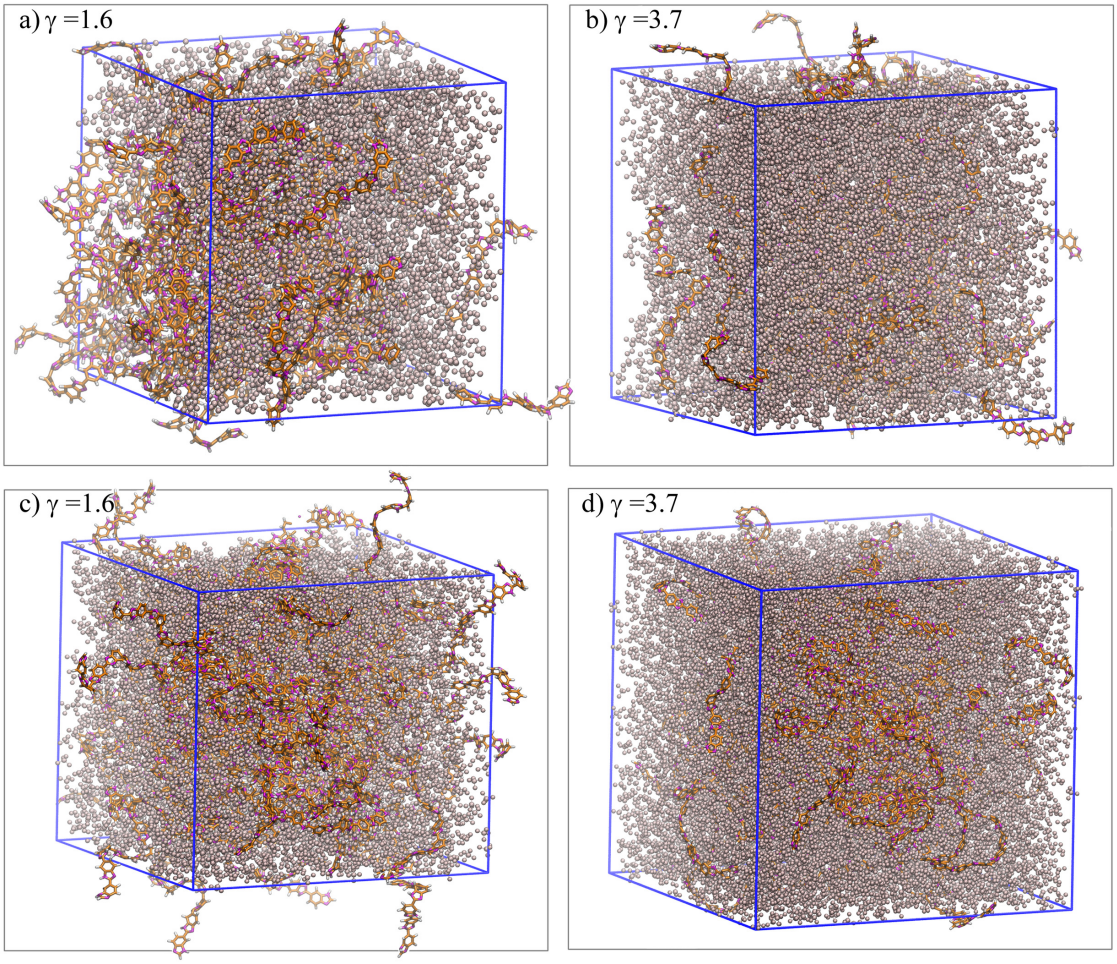

Figure B3-2: Snapshots of PA doped ABPBI membrane at 300 K from production run (a,b) for pentamer and (c,d) for decamer at γ = 1.6 and γ = 3.7 respectively. [ABPBI membrane = Licorice and PA molecule = CPK (Hydrogen atoms were not displayed)]

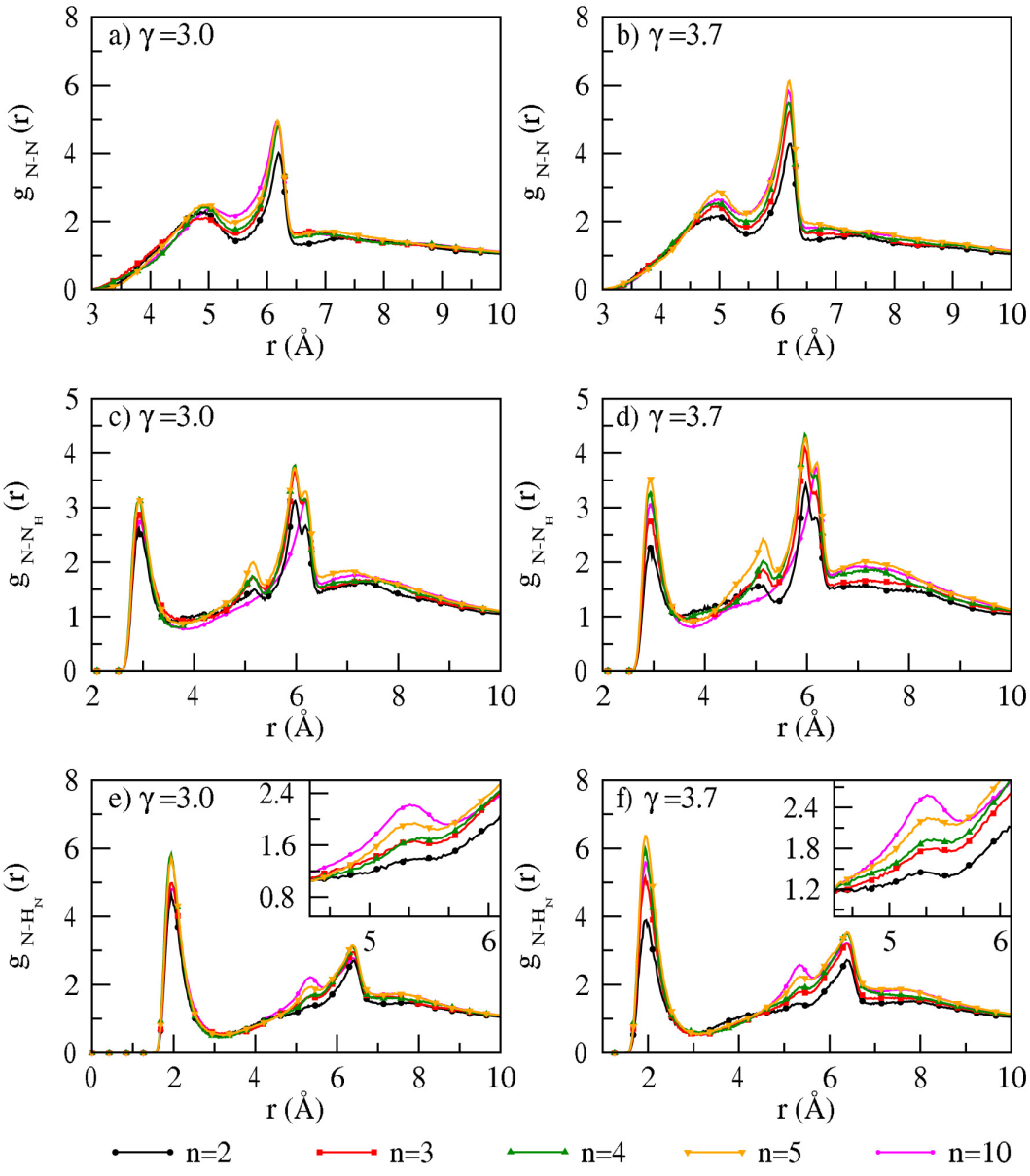

Figure B3-3: RDFs from (a,b) N-N, (c,d) N-N_H and (e,f) N-H_N interactions at T = 300 K and γ = 3.0 and 3.7.

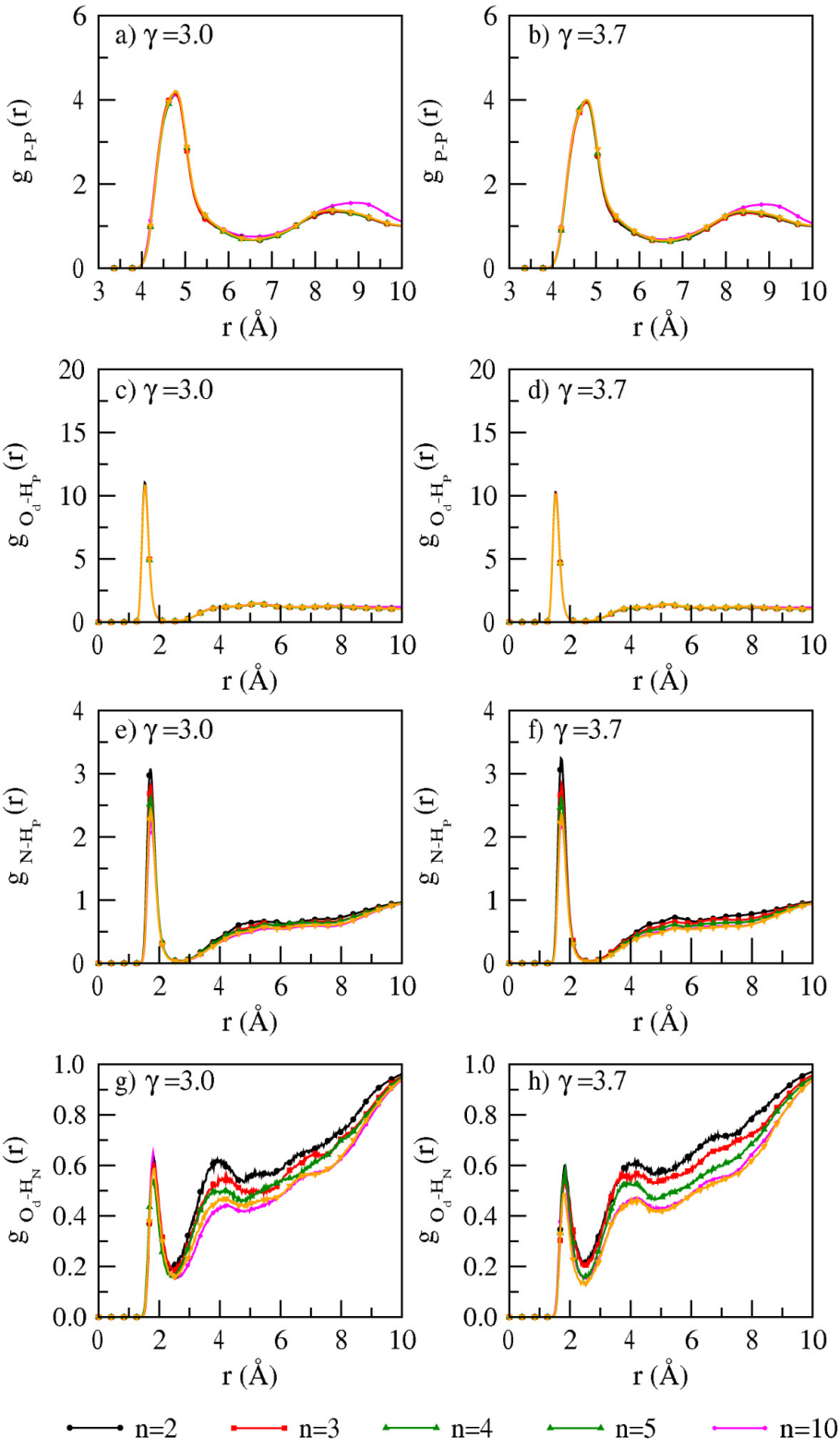

Figure B3-4: RDFs from (a,b) P-P, (c,d) O_d-H_P, (e,f) N-H_P and (g,h) O_d-H_N interactions at T = 300 K and γ = 3.0 and 3.7.

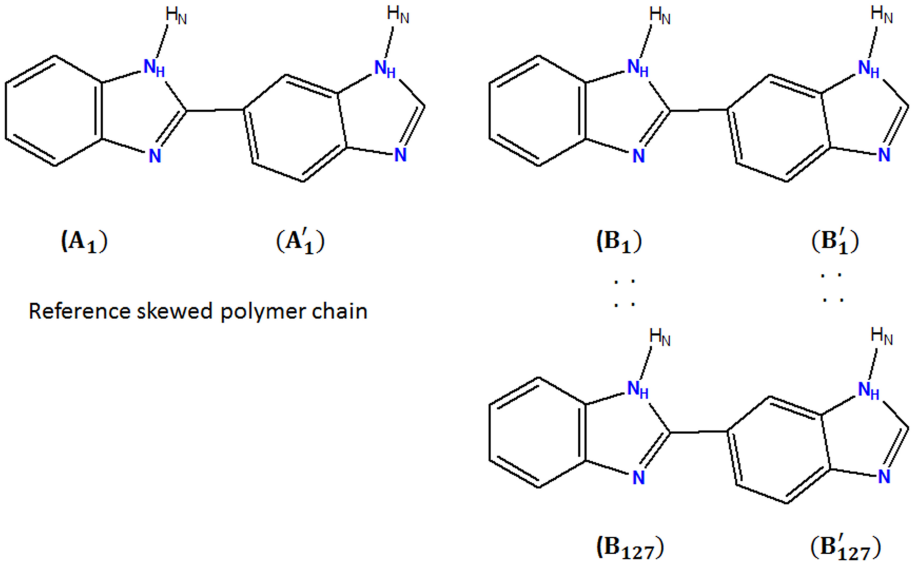

Figure B3-5: The BI_{com}-BI_{com} RDF is calculated using an average of RDFs in following manner: first choose a skewed configuration (lowest R_g) as a reference polymer chain. Each BI_{com}-BI_{com} RDF is calculated between the center of mass of a BI unit of the reference polymer chain and the center of mass of every BI unit of all other polymer chains. For e. g. in a dimer, the BI_{com}-BI_{com} RDF is calculated between the center of mass of each BI unit of the reference polymer chain and the center of mass of each BI unit of 127 ABPBI polymer chains. This leads to four possibilities of RDFs such as: (A1, B1-127), (A1, B′1-127), (A′1, B1-127), (A′1, B′1-127). Thus, the final BI_{com}-BI_{com} RDF is calculated from an average of these four BI_{com}-BI_{com} RDFs in a dimer. Similarly, the BI_{com}-BI_{com} RDFs in a trimer, tetramer, pentamer, and decamer is calculated as an average of 9, 16, 25 and 100 BI_{com}-BI_{com} RDFs respectively.

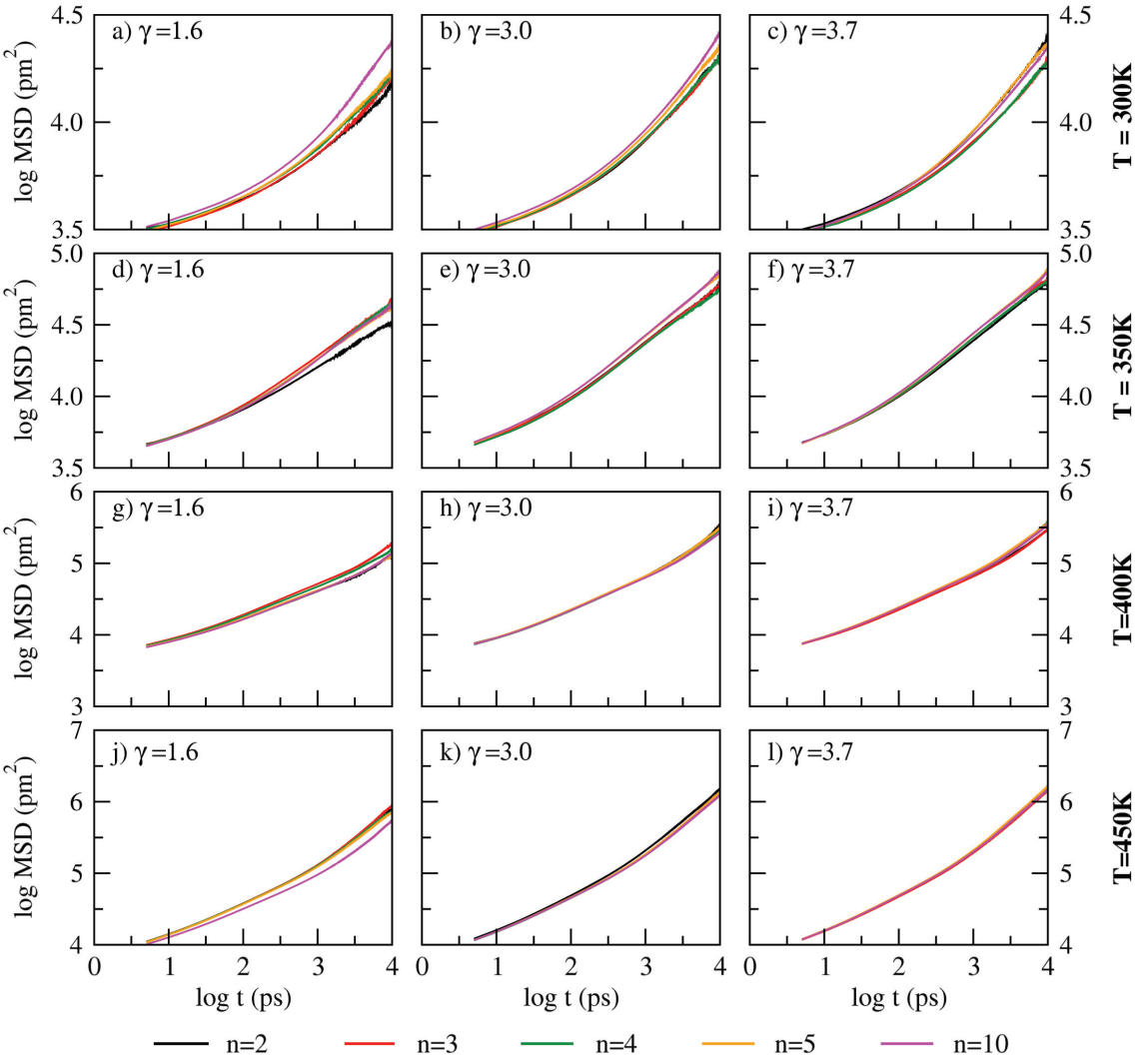

Figure B3-6: MSD of PA at a-c) 300 K, d-f) 350 K, g-i) 400 K and j-l) 450 K.

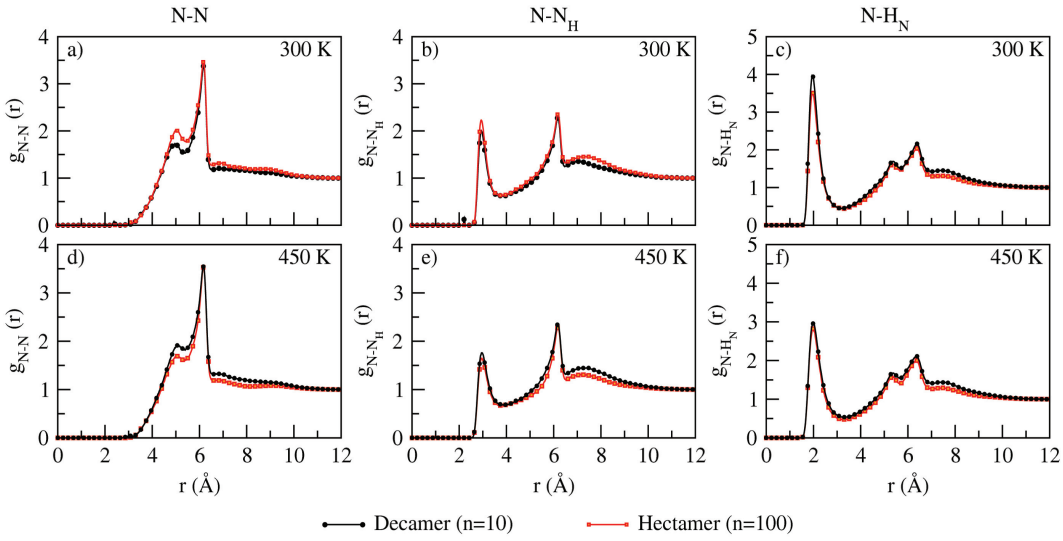

Figure B3-7: RDFs of imidazole interactions (N-N, N-N_H and N-H_N) at a-c) 300 K and d-f) 450 K for Decamer and Hectamer respectively.

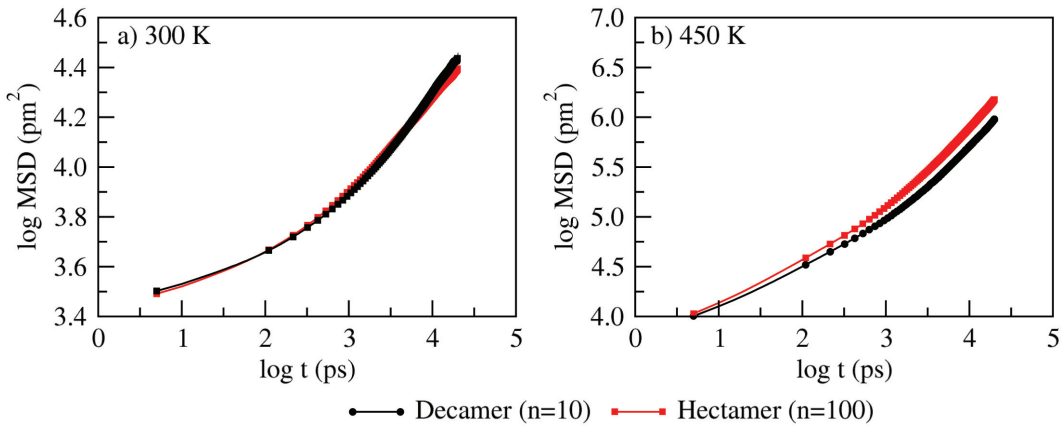

Figure B3-8: MSD of PA at a) 300 K and b) 450 K for Decamer and Hectamer respectively.

Bibliography

[1] Dresselhaus, M. S.; Thomas, I. L. *Nature* **2001**, *414*, 332–337.

[2] Steele, B. C. H.; Heinzel, A. *Nature* **2001**, *414*, 345–352.

[3] Kreuer, K.-D.; Paddison, S. J.; Spohr, E.; Schuster, M. *Chem. Rev.* **2004**, *104*, 4637–4678.

[4] Mauritz, K. A.; Moore, R. B. *Chem. Rev.* **2004**, *104*, 4535–4586.

[5] Hickner, M. A.; Ghassemi, H.; Kim, Y. S.; Einsla, B. R.; McGrath, J. E. *Chem. Rev.* **2004**, *104*, 4587–4612.

[6] Kreuer, K.-D. *Solid State Ionics* **1997**, *97*, 1–15.

[7] Kreuer, K.-D. *J. Membr. Sci.* **2001**, *185*, 29–39.

[8] Wang, Q.; Keffer, D. J.; Deng, S.; Mays, J. *Polymer* **2012**, *53*, 1517–1528.

[9] Wang, Q.; Suraweera, N. S.; Keffer, D. J.; Deng, S.; Mays, J. *Macromolecules* **2012**, *45*, 6669–6685.

[10] Asensio, J. A.; Borrs, S.; Gmez-Romero, P. *J. Polym. Sci., Part A: Polym. Chem.* **2002**, *40*, 3703–3710.

[11] Paddison, S. J.; Elliott, J. A. *J. Phys. Chem. A* **2005**, *109*, 7583–7593.

[12] Paul, R.; Paddison, S. J. *J. Chem. Phys.* **2005**, *123*, 224704–224714.

[13] Cui, S.; Liu, J.; Selvan, M. E.; Keffer, D. J.; Edwards, B. J.; Steele, W. V. *J. Phys. Chem. B* **2007**, *111*, 2208–2218.

[14] Venkatnathan, A.; Devanathan, R.; Dupuis, M. *J. Phys. Chem. B* **2007**, *111*, 7234–7244.

[15] Brandell, D.; Karo, J.; Liivat, A.; Thomas, J. *J. Mol. Model.* **2007**, *13*, 1039–1046.

[16] Cui, S.; Liu, J.; Selvan, M. E.; Paddison, S. J.; Keffer, D. J.; Edwards, B. J. *J. Phys. Chem. B* **2008**, *112*, 13273–13284.

[17] Karo, J.; Aabloo, A.; Thomas, J. O.; Brandell, D. *J. Phys. Chem. B* **2010**, *114*, 6056–6064.

[18] Devanathan, R.; Dupuis, M. *Phys. Chem. Chem. Phys.* **2012**, *14*, 11281–11295.

[19] Clark Ii, J. K.; Paddison, S. J. *Solid State Ionics* **2012**, *213*, 83–91.

[20] Sunda, A. P.; Venkatnathan, A. *Soft Matter* **2012**, *8*, 10827–10836.

[21] Musto, P.; Karasz, F.; MacKnight, W. *Polymer* **1993**, *34*, 2934–2945.

[22] Asensio, J. A.; Sanchez, E. M.; Gomez-Romero, P. *Chem. Soc. Rev.* **2010**, *39*, 3210–3239.

[23] Li, Q.; He, R.; Jensen, J. O.; Bjerrum, N. J. *Chem. Mater.* **2003**, *15*, 4896–4915.

[24] Zhang, J.; Xie, Z.; Zhang, J.; Tang, Y.; Song, C.; Navessin, T.; Shi, Z.; Song, D.; Wang, H.; Wilkinson, D. P.; Liu, Z.-S.; Holdcroft, S. *J. Power Sources* **2006**, *160*, 872–891.

[25] Devanathan, R. *Energy Environ. Sci.* **2008**, *1*, 101–119.

[26] Quartarone, E.; Mustarelli, P. *Energy Environ. Sci.* **2012**, *5*, 6436–6444.

[27] Zhang, H.; Shen, P. K. *Chem. Rev.* **2012**, *112*, 2780–2832.

[28] Xing, B.; Savadogo, O. *J. New Mater. Electrochem. Syst.* **1999**, *2*, 095–101.

[29] Dippel, T.; Kreuer, K. D.; Lassègues, J. C.; Rodriguez, D. *Solid State Ionics* **1993**, *61*, 41–46.

[30] Schuster, M. F. H.; Meyer, W. H.; Schuster, M.; Kreuer, K. D. *Chem. Mater.* **2004**, *16*, 329–337.

[31] Asensio, J. A.; Borros, S.; Gomez-Romero, P. *J. Electrochem. Soc.* **2004**, *151*, A304–A310.

[32] Kim, H.-J.; Cho, S. Y.; An, S. J.; Eun, Y. C.; Kim, J.-Y.; Yoon, H.-K.; Kweon, H.-J.; Yew, K. H. *Macromol. Rapid Commun.* **2004**, *25*, 894–897.

[33] Asensio, J. A.; Borrós, S.; Gómez-Romero, P. *J. Membr. Sci.* **2004**, *241*, 89–93.

[34] Asensio, J. A.; Borrós, S.; Gómez-Romero, P. *Electrochim. Acta* **2004**, *49*, 4461–4466.

[35] Asensio, J. A.; Gómez-Romero, P. *Fuel Cells* **2005**, *5*, 336–343.

[36] Krishnan, P.; Park, J.-S.; Kim, C.-S. *J. Power Sources* **2006**, *159*, 817–823.

[37] Glezakou, V.-A.; Dupuis, M.; Mundy, C. J. *Phys. Chem. Chem. Phys.* **2007**, *9*, 5752–5760.

[38] Wannek, C.; Kohnen, B.; Oetjen, H. F.; Lippert, H.; Mergel, J. *Fuel Cells* **2008**, *8*, 87–95.

[39] Li, Q.; Jensen, J. O.; Savinell, R. F.; Bjerrum, N. J. *Prog. Polym. Sci.* **2009**, *34*, 449–477.

[40] Kondratenko, M. S.; Gallyamov, M. O.; Khokhlov, A. R. *Int. J. Hydrogen Energy* **2012**, *37*, 2596–2602.

[41] Rodriguez, D.; Jegat, C.; Trinquet, O.; Grondin, J.; Lassègues, J. *Solid State Ionics* **1993**, *61*, 195–202.

[42] Giffin, G. A.; Conti, F.; Lavina, S.; Majerus, A.; Pace, G.; Korte, C.; Lehnert, W.; Noto, V. D. *Int. J. Hydrogen Energy* **2014**, *39*, 2776 – 2784.

[43] Litt, M.; Ameri, R.; Wang, Y.; Savinell, R.; Wainwright, J. *MRS Proceedings* **1998**, *548*, 313–323.

[44] Agmon, N. *Chem. Phys. Lett.* **1995**, *244*, 456–462.

[45] Diaz, L. A.; Abuin, G. C.; Corti, H. R. *J. Power Sources* **2009**, *188*, 45–50.

[46] Linares, J. J.; Sanches, C.; Paganin, V. A.; González, E. R. *J. Electrochem. Soc.* **2012**, *159*, F194–F202.

[47] Conti, F.; Majerus, A.; Di Noto, V.; Korte, C.; Lehnert, W.; Stolten, D. *Phys. Chem. Chem. Phys.* **2012**, *14*, 10022–10026.

[48] Li, S.; Fried, J. R.; Colebrook, J.; Burkhardt, J. *Polymer* **2010**, *51*, 5640–5648.

[49] Allen, M.; Tildesley, D. *Computer Simulation of Liquids*; Oxford Science Publications; Clarendon Press, **1989**.

[50] Leach, A. *Molecular Modelling: Principles and Applications*; Pearson Education; Prentice Hall, 2001.

[51] MacKerell, A. D. et al. *J. Phys. Chem. B* **1998**, *102*, 3586–3616, PMID: 24889800.

[52] Cornell, W. D.; Cieplak, P.; Bayly, C. I.; Gould, I. R.; Merz, K. M.; Ferguson, D. M.; Spellmeyer, D. C.; Fox, T.; Caldwell, J. W.; Kollman, P. A. *J. Am. Chem. Soc.* **1995**, *117*, 5179–5197.

[53] Jorgensen, W. L.; Maxwell, D. S.; Tirado-Rives, J. *J. Am. Chem. Soc.* **1996**, *118*, 11225–11236.

[54] Schaftenaar, G.; Noordik, J. *J. Comput.Aided Mol. Design* **2000**, *14*, 123–134.

[55] Dennington, R.; Keith, T.; Millam, J. Semichem Inc. Shawnee Mission KS 2009.

[56] Humphrey, W.; Dalke, A.; Schulten, K. *J. Molecular Graphics* **1996**, *14*, 33 – 38.

[57] Pettersen, E. F.; Goddard, T. D.; Huang, C. C.; Couch, G. S.; Greenblatt, D. M.; Meng, E. C.; Ferrin, T. E. *J. Comput. Chem.* **2004**, *25*, 1605–1612.

[58] Payne, M. C.; Teter, M. P.; Allan, D. C.; Arias, T. A.; Joannopoulos, J. D. *Rev. Mod. Phys.* **1992**, *64*, 1045–1097.

[59] Sperling, L. *Introduction to Physical Polymer Science*; Wiley, **2005**.

[60] Hiemenz, P.; Lodge, T. *Polymer Chemistry, Second Edition*; Taylor & Francis, **2007**.

[61] Hess, B.; Kutzner, C.; van der Spoel, D.; Lindahl, E. *J. Chem. Theory Comput.* **2008**, *4*, 435–447.

[62] Jorgensen, W. L.; Tirado-Rives, J. *J. Am. Chem. Soc.* **1988**, *110*, 1657–1666.

[63] Spieser, S. A. H.; Leeflang, B. R.; Kroon-Batenburg, L. M. J.; Kroon, J. *J. Phys. Chem. A* **2000**, *104*, 7333–7338.

[64] Berendsen, H. J. C.; Postma, J. P. M.; van Gunsteren, W. F.; DiNola, A.; Haak, J. R. *J. Chem. Phys.* **1984**, *81*, 3684–3690.

[65] Bussi, G.; Donadio, D.; Parrinello, M. *J. Chem. Phys.* **2007**, *126*, 14101–14107.

[66] Darden, T.; York, D.; Pedersen, L. *J. Chem. Phys.* **1993**, *98*, 10089–10092.

[67] Essmann, U.; Perera, L.; Berkowitz, M. L.; Darden, T.; Lee, H.; Pedersen, L. G. *J. Chem. Phys.* **1995**, *103*, 8577–8593.

[68] Nosé, S. *Mol. Phys.* **1984**, *52*, 255–268.

[69] Hoover, W. G. *Phys. Rev. A* **1985**, *31*, 1695–1697.

[70] Parrinello, M. *J. Appl. Phys.* **1981**, *52*, 7182–7190.

[71] Nosé, S.; Klein, M. *Mol. Phys.* **1983**, *50*, 1055–1076.

[72] Vijayan, N.; Balamurugan, N.; Ramesh Babu, R.; Gopalakrishnan, R.; Ramasamy, P.; Harrison, W. *J. Cryst. Growth* **2004**, *267*, 218–222.

[73] Egan, E. P.; Luff, B. B. *Ind. Eng. Chem.* **1955**, *47*, 1280–1281.

[74] Tromp, R. H.; Spieser, S. H.; Neilson, G. W. *J. Chem. Phys.* **1999**, *110*, 2145–2150.

[75] Tsuchida, E. *J. Phys. Soc. Jpn.* **2006**, *75*, 054801–054805.

[76] Li, S.; Fried, J. R.; Sauer, J.; Colebrook, J.; Dudis, D. S. *Int. J. Quantum Chem* **2011**, *111*, 3212–3229.

[77] Stillinger, F. H. *Adv. Chem. Phys.*; John Wiley Sons, Inc., **2007**.

[78] Luzar, A.; Chandler, D. *Nature* **1996**, *379*, 55–57.

[79] van der Spoel, D.; van Maaren, P. J.; Larsson, P.; Tîmneanu, N. *J. Phys. Chem. B* **2006**, *110*, 4393–4398.

[80] Luzar, A.; Chandler, D. *J. Chem. Phys.* **1993**, *98*, 8160–8173.

[81] Starr, F. W.; Nielsen, J. K.; Stanley, H. E. *Phys. Rev Lett.* **1999**, *82*, 2294–2297.

[82] Starr, F. W.; Nielsen, J. K.; Stanley, H. E. *Phys. Rev. E* **2000**, *62*, 579–87.

[83] Sunda, A. P.; More, M.; Venkatnathan, A. *Soft Matter* **2013**, *9*, 1122–1132.

[84] Jorgensen, W. L.; Maxwell, D. S.; Tirado-Rives, J. *J. Am. Chem. Soc.* **1996**, *118*, 11225–11236.

[85] Hwang, W. F.; Wiff, D. R.; Verschoore, C.; Price, G. E.; Helminiak, T. E.; Adams, W. W. *Polym. Eng. Sci.* **1983**, *23*, 784–788.

[86] Glipa, X.; Bonnet, B.; Mula, B.; J. Jones, D.; Roziere, J. *J. Mater. Chem.* **1999**, *9*, 3045–3049.

[87] Ma, Y. L.; Wainright, J. S.; Litt, M. H.; Savinell, R. F. *J. Electrochem. Soc.* **2004**, *151*, A8–A16.

[88] Kim, S.-K.; Ko, T.; Choi, S.-W.; Park, J. O.; Kim, K.-H.; Pak, C.; Chang, H.; Lee, J.-C. *J. Mater. Chem.* **2012**, *22*, 7194–7205.

[89] Edwards, S. F. *Proc. Phys. Soc.* **1966**, *88*, 265–280.

[90] Daoud, M.; Cotton, J. P.; Farnoux, B.; Jannink, G.; Sarma, G.; Benoit, H.; Duplessix, C.; Picot, C.; de Gennes, P. G. *Macromolecules* **1975**, *8*, 804–818.

[91] de Gennes, P. *Scaling Concepts in Polymer Physics*; Cornell University Press, **1979**.

[92] Laso, M.; Karayiannis, N. C. *J. Chem. Phys.* **2008**, *128*, 174901.

[93] Wang, Q.; Keffer, D. J.; Petrovan, S.; Thomas, J. B. *J. Phys. Chem. B* **2009**, *114*, 786–795.

[94] Wang, Q.; Keffer, D. J.; Nicholson, D. M.; Thomas, J. B. *Macromolecules* **2010**, *43*, 10722–10734.

[95] Daura, X.; Gademann, K.; Jaun, B.; Seebach, D.; van Gunsteren, W. F.; Mark, A. E. *Angew. Chem. Int. Ed.* **1999**, *38*, 236–240.

[96] Hunter, C. A.; Sanders, J. K. M. *J. Am. Chem. Soc.* **1990**, *112*, 5525–5534.

[97] Sacksteder, C. A.; Bender, S. L.; Barry, B. A. *J. Am. Chem. Soc.* **2005**, *127*, 7879–7890.

[98] Plevin, M. J.; Bryce, D. L.; Boisbouvier, J. *Nat. Chem.* **2010**, *2*, 466–471.

[99] Tsuzuki, S. *Annu. Rep. Prog. Chem. Sect. C: Phys. Chem.* **2012**, *108*, 69–95.

[100] Ye, H.; Huang, J.; Xu, J. J.; Kodiweera, N.; Jayakody, J. R. P.; Greenbaum, S. G. *J. Power Sources* **2008**, *178*, 651–660.

[101] Shen, C.-H.; chung Hsu, S. L.; Bulycheva, E.; Belomoina, N. *J. Membr. Sci.* **2012**, *399–400*, 11–15.

[102] Mishra, A. K.; Kim, N. H.; Lee, J. H. *J. Membr. Sci.* **2014**, *449*, 136–145.

[103] Noda, A.; Hayamizu, K.; Watanabe, M. *J. Phys. Chem. B* **2001**, *105*, 4603–4610.

[104] Nakamoto, H.; Watanabe, M. *Chem. Commun.* **2007**, 2539–2541.

[105] Greaves, T. L.; Drummond, C. J. *Chem. Rev.* **2008**, *108*, 206–237.

[106] Yasuda, T.; Watanabe, M. *MRS Bulletin* **2013**, *38*, 560–566.

[107] Lee, S.-Y.; Ogawa, A.; Kanno, M.; Nakamoto, H.; Yasuda, T.; Watanabe, M. *J. Am. Chem. Soc.* **2010**, *132*, 9764–9773.

[108] Yasuda, T.; Nakamura, S.-i.; Honda, Y.; Kinugawa, K.; Lee, S.-Y.; Watanabe, M. *ACS Appl. Mater. Interfaces* **2012**, *4*, 1783–1790.

[109] Chang, T. M.; Dang, L. X.; Devanathan, R.; Dupuis, M. *J. Phys. Chem. A* **2010**, *114*, 12764–12774.

[110] Johnson, L.; Ejigu, A.; Licence, P.; Walsh, D. A. *J. Phys. Chem. C* **2012**, *116*, 18048–18056.

[111] Liu, S.; Zhou, L.; Wang, P.; Zhang, F.; Yu, S.; Shao, Z.; Yi, B. *ACS Appl. Mater. Interfaces* **2014**, *6*, 3195–3200.

[112] Marx, D.; Hutter, J. *Ab Initio Molecular Dynamics: Basic Theory and Advanced Methods*; Cambridge University Press, **2009**.